The Company of
Biologists

STEM CELLS AND REGENERATION

RESEARCH ARTICLE

Single cell dynamics of embryonic muscle progenitor cells in zebrafish

Priyanka Sharma[1], Tyler D. Ruel[1], Katrinka M. Kocha[1], Shan Liao[2] and Peng Huang[1],*

ABSTRACT

Muscle stem cells hold a great therapeutic potential in regenerating damaged muscles. However, the *in vivo* behavior of muscle stem cells during muscle growth and regeneration is still poorly understood. Using zebrafish as a model, we describe the *in vivo* dynamics and function of embryonic muscle progenitor cells (MPCs) in the dermomyotome. These cells are located in a superficial layer external to muscle fibers and express many extracellular matrix (ECM) genes, including *collagen type 1 α2* (*col1a2*). Utilizing a new *col1a2* transgenic line, we show that *col1a2*+ MPCs display a ramified morphology with dynamic cellular processes. Cell lineage tracing demonstrates that *col1a2*+ MPCs contribute to new myofibers in normal muscle growth and also during muscle regeneration. A combination of live imaging and single cell clonal analysis reveals a highly choreographed process of muscle regeneration. Activated *col1a2*+ MPCs change from the quiescent ramified morphology to a polarized and elongated morphology, generating daughter cells that fuse with existing myofibers. Partial depletion of *col1a2*+ MPCs severely compromises muscle regeneration. Our work provides a dynamic view of embryonic muscle progenitor cells during zebrafish muscle growth and regeneration.

KEY WORDS: Dermomyotome, Somite, Muscle progenitor cells, *In vivo* imaging, Extracellular matrix, Zebrafish

INTRODUCTION

Tissue-resident stem cells, such as muscle stem cells, are crucial for proper organ development and tissue homeostasis. To harness the power of stem cells for treating diseases such as muscular dystrophy, it is critical to understand how muscle progenitor cells (MPCs) behave *in vivo*. In vertebrates, many skeletal muscles originate from the somites (Saga and Takeda, 2001). As the embryo develops, the ventral somite forms the sclerotome, generating progenitors of the axial skeleton and tendons, whereas the dorsolateral somite forms the dermomyotome. The dermomyotome further splits to form the dermatome and the myotome, which contribute to the skin and skeletal muscles, respectively (Christ and Scaal, 2008; Scaal and Christ, 2004). Thus, the dermomyotome contains embryonic MPCs required for the initial formation and growth of the musculature. Fate mapping and lineage tracing experiments in mouse and chick have

demonstrated that the dermomyotome is also the source of adult muscle stem cells known as satellite cells (Gros et al., 2005; Kassar-Duchossoy et al., 2005; Relaix et al., 2005; Schienda et al., 2006).

Both embryonic MPCs in the dermomyotome and satellite cells contribute to myofiber formation, and are marked by the expression of the paired box transcription factors *Pax3* and *Pax7* (Dumont et al., 2015; Scaal and Christ, 2004). However, the function and dynamics of satellite cells have been more extensively studied than embryonic MPCs. Quiescent satellite cells often display a bipolar morphology and reside beneath the basal lamina on the surface of the myofiber (Scharner and Zammit, 2011; Webster et al., 2016). The extracellular matrix (ECM) surrounding the satellite cell constitutes its niche and has been implicated in the regulation of satellite cell behavior (Baghdadi et al., 2018; Bentzinger et al., 2013b; Fry et al., 2017; Rayagiri et al., 2018; Tierney et al., 2016; Urciuolo et al., 2013). Upon muscle injury, 'activated' satellite cells undergo proliferation and initiate the myogenic program. The sequential production of myogenic regulatory factors, including Myf5, MyoD and Myogenin, results in the differentiation of myoblasts that align and form new syncytial myofibers or fuse with existing myofibers. A single transplanted satellite cell is capable of self-renewal and contributes to myofibers (Sacco et al., 2008). Conversely, genetic ablation of satellite cells in adult mice completely abolishes injury-induced muscle regeneration (Lepper et al., 2011; Murphy et al., 2011; Sambasivan et al., 2011), demonstrating a critical role of satellite cells in muscle regeneration.

It has been challenging to visualize the *in vivo* behavior of satellite cells. Previous work has been mostly inferred from 'snapshots' of histological sections or analysis from *in vitro* cultures (Bentzinger et al., 2014; El Fahime et al., 2000; Jockusch and Voigt, 2003; Kuang et al., 2007; Siegel et al., 2009). However, satellite cells that are separated from their physiological environment are invariably activated, and *in vitro* approaches do not therefore provide the whole picture of their endogenous behavior. With the advance of intravital imaging, recent work provides the first glimpse of mouse satellite cell behavior *in vivo* (Webster et al., 2016). Quiescent satellite cells are largely immobile, whereas activated satellite cells proliferate and migrate along the ECM remnants of injured myofibers during regeneration.

The remarkable regenerative ability and the ease of *in vivo* imaging have made zebrafish a powerful system to study MPC behavior (Ratnayake and Currie, 2017). Muscle injury can be 'repaired' by resealing the membrane of the damaged myofiber or 'regenerated' by replacing the damaged muscle with a new myofiber generated by MPCs. In this study, we focus on muscle regeneration by MPCs. The zebrafish dermomyotome, also known as the external cell layer (ECL), is marked by the expression of *pax3* and *pax7*, similar to higher vertebrates (Devoto et al., 2006; Feng et al., 2006; Hammond et al., 2007). During somitogenesis, the *pax3/pax7*+ dermomyotome is generated from the anterior somitic compartment via whole-somite rotation and is thought to generate new myofibers

[1]Department of Biochemistry and Molecular Biology, Cumming School of Medicine, Alberta Children's Hospital Research Institute, University of Calgary, 3330 Hospital Drive, Calgary, AB T2N 4N1, Canada. [2]Inflammation Research Network, The Snyder Institute for Chronic Diseases, Department of Microbiology, Immunology and Infectious Diseases, Cumming School of Medicine, University of Calgary, 3330 Hospital Drive, Calgary, AB T2N 4N1, Canada.

*Author for correspondence (huangp@ucalgary.ca)

S.L., 0000-0002-9094-5846; P.H., 0000-0001-7954-8869

DEVELOPMENT

during myotome growth (Hollway et al., 2007; Stellabotte et al., 2007). At 4-5 days post-fertilization (dpf), some $pax7^+$ MPCs derived from the dermomyotome can be observed deep in the myotome between myofibers (Seger et al., 2011). A sub-population of these $pax7^+$ fiber-associated cells is specifically marked by the mouse satellite cell marker $cmet$. $cmet^+$ cells are capable of self-renewal and contribute to muscle regeneration, suggesting that they are functionally equivalent to mammalian satellite cells (Gurevich et al., 2016). Recent work has also shown that Pax3/7-expressing satellite-like cells in adult zebrafish are essential for the regeneration after muscle injury (Berberoglu et al., 2017). Therefore, $pax7$ labels multiple MPC populations at different developmental stages in zebrafish: (1) embryonic MPCs in the dermomyotome on the surface of the somite; (2) fiber-associated deep myotomal cells (including $cmet^+$ cells) in larval zebrafish; and (3) satellite-like cells in adult zebrafish.

To understand how embryonic MPCs contribute to muscle regeneration, we developed new transgenic tools and methods to analyze their dynamics and function at single cell resolution. We identified several ECM genes as new markers of embryonic MPCs. Genetic lineage tracing using $col1a2$-based transgenic lines demonstrated that $col1a2^+$ MPCs contribute not only to embryonic muscle growth but also to muscle regeneration after injury. Combining in $vivo$ imaging and single cell clonal analysis, we describe the dynamics of 'quiescent' and 'activated' $col1a2^+$ MPCs. Together, our study provides a dynamic view of embryonic MPCs during muscle growth and regeneration.

RESULTS
Embryonic MPCs express many extracellular matrix genes
Embryonic MPCs in the dermomyotome in zebrafish are traditionally labeled by the expression of $pax7a$ (Devoto et al., 2006; Feng et al., 2006; Hammond et al., 2007). Using double fluorescent in $situ$ hybridization, we identified several extracellular matrix (ECM) genes, including $col1a2$ ($collagen$ $type$ 1 $α2$), $col5a1$ ($collagen$ $type$ 5 $α1$) and $cilp$ ($cartilage$ $intermediate$ $layer$ $protein$), that showed co-expression with $pax7a$ on the outer surface of the somite (Fig. 1A). To visualize embryonic MPC dynamics in $vivo$, we generated a $col1a2:Gal4$ transgenic line by BAC recombineering (Fig. 1B). The $col1a2:Gal4$ line can be crossed with different UAS effector lines to label, ablate or lineage trace MPCs. Co-labeling using $col1a2$ and $kaede$ probes in $col1a2:Gal4;$ $UAS:Kaede$ ($col1a2^{Kaede}$) embryos revealed that the $col1a2:Gal4$ reporter largely recapitulated the endogenous $col1a2$ expression pattern (Fig. S1). Similarly, $col1a2:Gal4;$ $UAS:NTR-mCherry$ ($col1a2^{NTR-mCherry}$) labeled the outer surface of the somite external to $α$-$actin:GFP$-expressing muscle cells, corresponding to the anatomical location of the dermomyotome (Fig. 1C; Movie 1). To determine whether the $col1a2:Gal4$ line labels embryonic MPCs, we performed immunostaining using an anti-Pax7 antibody in $col1a2^{NTR-mCherry}$ embryos. At 2 dpf, Pax7 antibody labels both MPCs (weak staining) and xanthophores, neural crest-derived pigment cells (strong staining). Indeed, all $mCherry^+$ cells on the lateral surface of the somite were weakly $Pax7^+$ (Fig. 1D), indicating that $col1a2^{NTR-mCherry}$ specifically labels MPCs in the dermomyotome but not xanthophores. On average, there were 24.6 $Pax7^+$ MPCs on the superficial surface of each somite, of which ~87% were also $mCherry^+$ (Fig. S2A). The incomplete labeling might be because gene expression driven by the Gal4-UAS system is variegated (Akitake et al., 2011), or alternatively, the $col1a2:Gal4$ line might label a sub-population of $Pax7^+$ MPCs. At 5 dpf, $Pax7^+$ fiber-associated

MPCs (about 9.3 per somite) started to emerge in the deep myotome, of which about 39% were weakly $mCherry^+$, probably due to the perdurance of the mCherry protein (Fig. 1D; Fig. S2B). Based on marker expression and lineage analysis (shown later), we termed $Pax7^+col1a2^+$ cells on the superficial surface of the somite '$col1a2^+$ MPCs'. In this study, we focused on the behavior and function of such $col1a2^+$ MPCs.

To determine whether the dermomyotome on the surface of muscles persists in adult zebrafish, we imaged vibratome sections of $col1a2^{NTR-mCherry}$ fish at 22 mm standard length (SL). We identified three layers of $col1a2^+$ cells external to the muscles, corresponding to scales (the most outer layer), skin (the middle layer) and the presumptive dermomyotome (the innermost layer external to muscles) (Fig. 1E). The presence of a few weakly $mCherry^+$ myofibers adjacent to the presumptive dermomyotome suggests that $col1a2^+$ cells contribute to muscle growth in adult zebrafish.

Characterization of $col1a2^+$ MPCs
Using the $col1a2:Gal4$ line, we determined the distribution, morphology and dynamics of $col1a2^+$ MPCs. First, we quantified the distribution of $col1a2^+$ MPCs in $col1a2^{NTR-mCherry}$ embryos stained with the Pax7 antibody at 2 dpf. Most $col1a2^+$ MPCs were located along the myosepta with 42% along the vertical myoseptum (VM) and 15% along the horizontal myoseptum (HM) (Fig. 1D; Fig. 2A,B). Second, by taking advantage of some highly mosaic $col1a2^{Kaede}$ embryos (which probably result from transcriptional silencing of UAS repeats over many generations; Akitake et al., 2011), we were able to visualize the morphology of individual $col1a2^+$ MPCs at 3 dpf (Fig. 2C). They were relatively flat cells sandwiched between the epidermis and myofibers. Individual $col1a2^+$ MPCs appeared to either 'float' in between the two somite boundaries or 'anchor' their cell bodies along the myoseptum. They always exhibited a ramified morphology with multipolar lamellipodia-like cellular projections (Fig. 2C). Thin filopodia-like projections (up to 25 μm) extending out of these lamellipodia can often be observed in $col1a2^+$ MPCs, suggesting potential long-range cell-cell communications or the ability to detect distant injuries. Quantification showed that $col1a2^+$ MPCs along the HM displayed fewer filopodia compared with cells along the VM, whereas centrally located MPCs had shorter filopodia than cells along the VM and HM (Fig. S2C,D). By combining two UAS reporters, we next visualized the dynamics of $col1a2^+$ MPCs in $col1a2:Gal4;$ $UAS:NTR-mCherry;$ $UAS:Kaede$ embryos (Fig. 2D). The mosaic nature of these transgenes allowed us to label a large number of $col1a2^+$ MPCs in different colors. $col1a2^+$ MPCs appeared to cover the surface of the somite with each cell occupying a non-overlapping territory. Time-lapse imaging showed that after cell division, daughter cells regained the ramified morphology and maintained the similar territory previously occupied by the mother cell (Fig. 2D; Movie 2). Together, our results demonstrate that the new $col1a2:Gal4$ line can be utilized to visualize the dynamics of embryonic MPCs at single cell resolution.

$col1a2^+$ MPCs generate new myofibers during muscle growth
To determine whether $col1a2^+$ MPCs contribute to muscle growth, we performed Cre-mediated lineage tracing to determine the fate of $col1a2^+$ MPCs. We generated the $col1a2:Gal4;$ $UAS:Cre-ERT2$ ($col1a2^{Cre-ERT2}$) transgenic line to express tamoxifen-inducible Cre recombinase in $col1a2^+$ cells, and utilized the $ubi:loxP-EGFP-loxP-mCherry$ ($ubi:Switch$) line (Mosimann et al., 2011) as the lineage reporter. Induction of Cre activity by 4-hydroxytamoxifen (4-OHT) results in the excision of the EGFP cassette and permanent
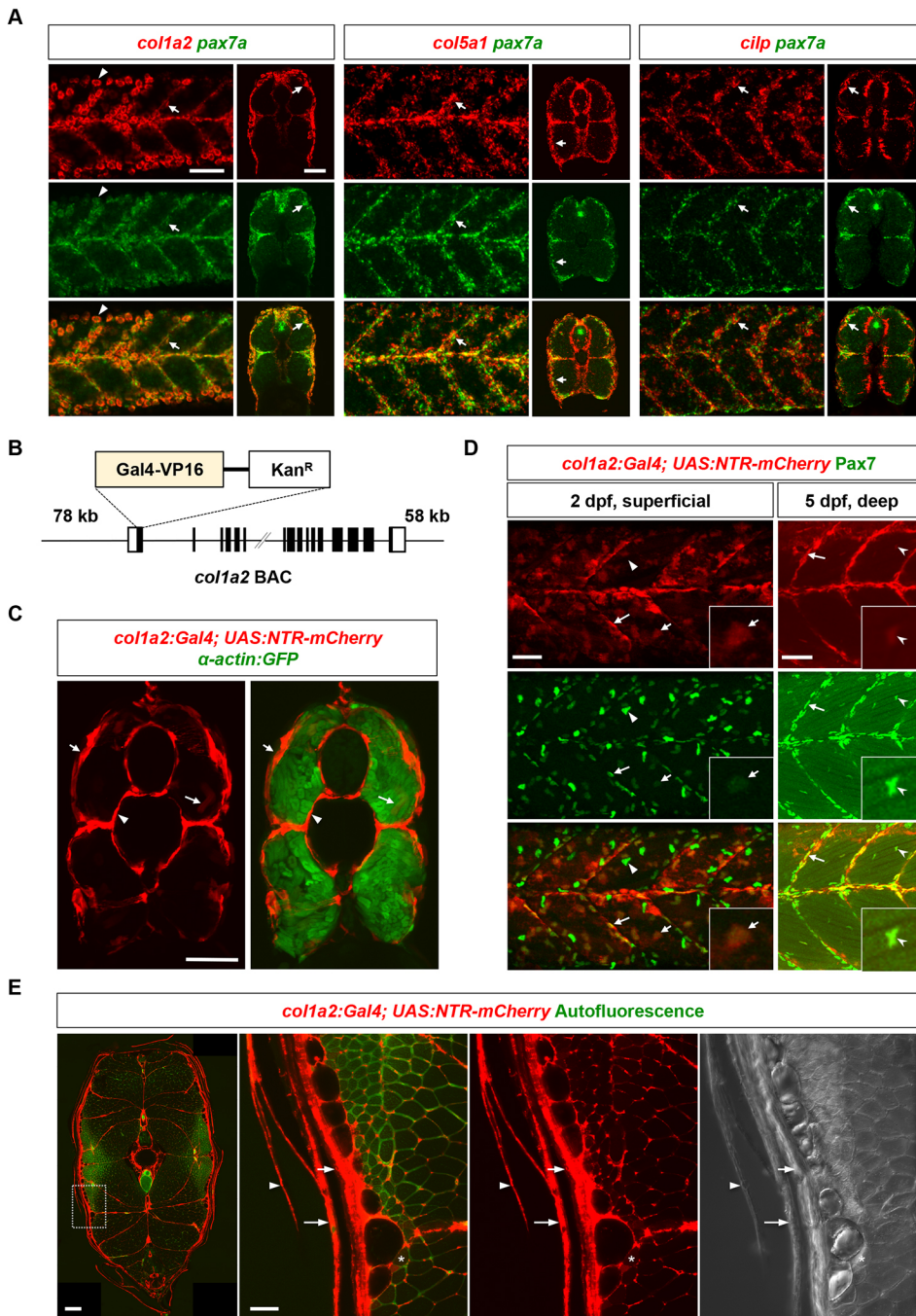
Fig. 1. The dermomyotome is marked by the expression of ECM genes. (A) Double fluorescent *in situ* hybridization shows the co-expression of ECM genes *col1a2*, *col5a1* and *cilp* (red) with the MPC marker *pax7a* (green) in the dermomyotome (arrows) at 3 dpf. Both lateral and transverse views are shown. Note that the high level of *col1a2* expression in the epidermis bleeds into the green channel (arrowheads). *n*=13 embryos per staining. (B) Schematics of the *col1a2: Gal4* BAC reporter. (C) *col1a2^{NTR-mCherry}; α-actin:GFP* fish at 3 dpf shows mCherry expression (red) in the dermomyotome (short arrows) on the surface of muscles, labeled by *α-actin:GFP* (green), cells around the notochord (arrowheads) and occasionally myofibers (long arrows). *n*=16 embryos. (D) *col1a2^{NTR-mCherry}* fish (red) were co-stained with the anti-Pax7 antibody (green). At 2 dpf, a superficial plane shows that most *mCherry^+* cells are co-labeled with Pax7 (*n*=20 embryos). Note that Pax7 also labels *mCherry^−* xanthophores (bean-shaped nuclei with stronger Pax7 staining, arrowheads). At 5 dpf, a deeper plane shows that some *Pax7^+* fiber-associated MPCs are weakly *mCherry^+* (*n*=37 embryos). Insets show magnified views of double positive MPCs. Long arrows: MPCs along the vertical myoseptum; short arrows: centrally located MPCs; notched arrowheads: fiber-associated MPCs. (E) Stitched confocal tile scans show transverse views of *col1a2^{NTR-mCherry}* fish at 22 mm SL. Expanded views of the boxed region are shown on the right. mCherry expression (red) can be observed in the presumptive dermomyotome (short arrows), the skin (long arrows), scales (arrowheads) and occasionally muscles (asterisks). The autofluorescence signal (green) is shown to highlight the outline of myofibers. *n*=6 fish. Scale bars: 50 μm (A,C,D,E) and 200 μm (left panel in E).

expression of the mCherry protein in the Cre-expressing cell and its progeny (Fig. 3A). *col1a2^{Cre-ERT2}; ubi:Switch* embryos were pulsed with 4-OHT for 2 h at 3 dpf to mosaicly label *col1a2^+* MPCs, and the mosaicism allows for reliable cell tracing over multiple time points. At 24 h after the 4-OHT pulse, a small fraction of *col1a2^+* MPCs on the surface of the somite was labeled by the mCherry expression, but no myofibers were labeled (Fig. 3B). Tracing of *mCherry^+* MPCs for 4 consecutive days revealed that new *mCherry^+* myofibers started to emerge at 48 h after 4-OHT pulse, and increased in number at later time points. Similar results were obtained with photoconversion-based lineage tracing experiments in *col1a2^{Kaede}* embryos (Fig. S3A,B). These results indicate that *col1a2^+* cells, most likely *col1a2^+* MPCs, contribute to the generation of new myofibers during larval muscle growth. Long-

term tracing of *col1a2^+* cells resulted in substantial labeling of the skin and muscles in fish at 4 weeks post-fertilization (wpf) and 1 year post-fertilization (ypf) (Fig. 3C). Interestingly, almost all *mCherry^+* myofibers were also *GFP^+*. By contrast, 'switched' skin cells were mostly *mCherry^+GFP^−*. This observation suggests that *col1a2^+* MPCs contribute to muscle growth by cell fusion in adult zebrafish.

ECM dynamics during muscle regeneration

Since *col1a2^+* MPCs contribute to muscle growth, we next asked whether they also contribute to muscle regeneration. We performed needle injury experiments on muscles of *col1a2^{NTR-mCherry}; α-actin:GFP* embryos (Fig. 4A). Fish were injured within a 1-2 somite area at 3 dpf and imaged every 24 h for 3 days. The
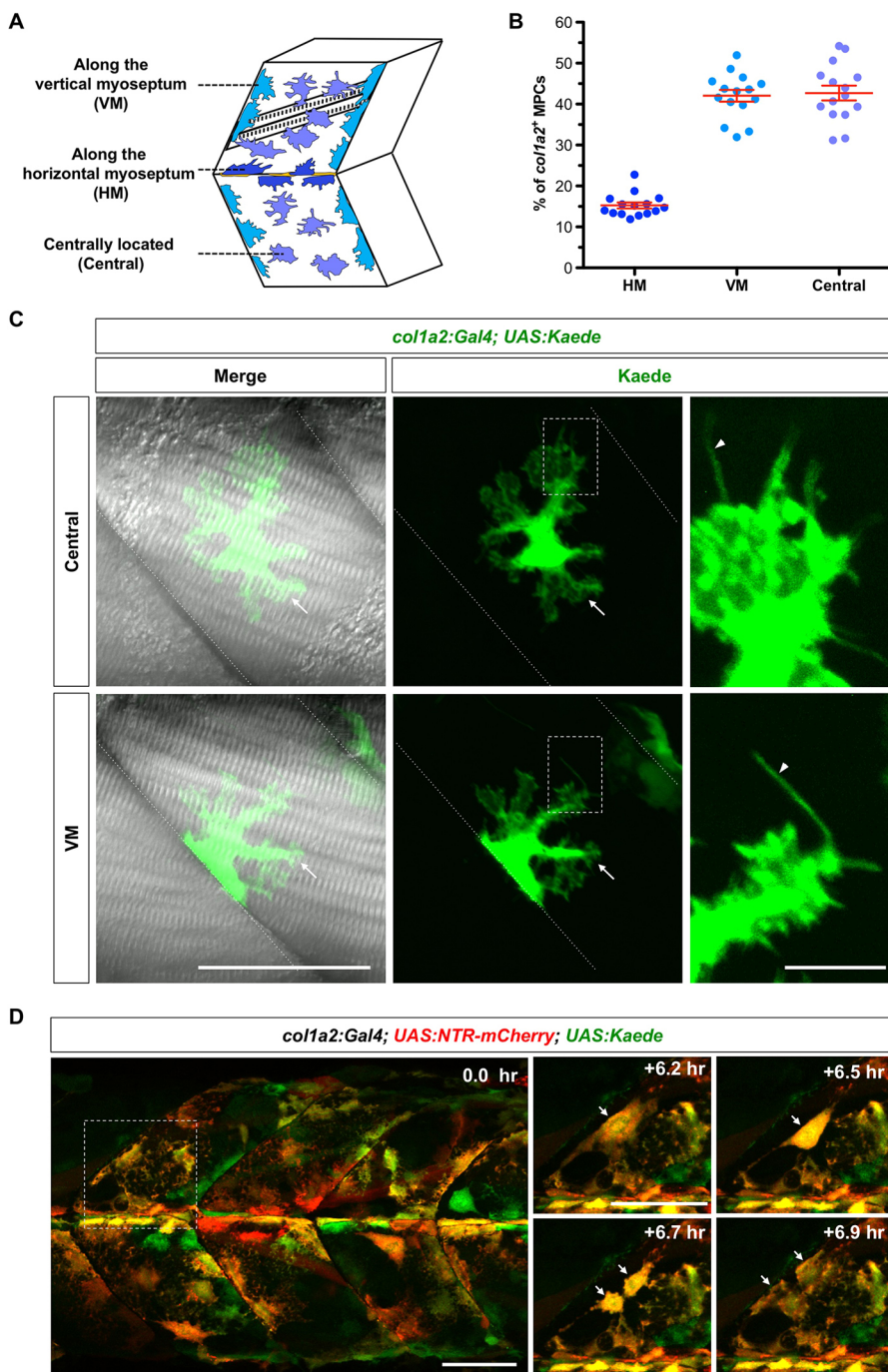
3

Fig. 2. Characterization of *col1a2*+ MPCs.
(A) Schematics of *col1a2*+ MPC distribution.
(B) Quantification of *col1a2*+ MPC distribution at 2 dpf. *n*=15 embryos. (C) Mosaic *col1a2*^Kaede^ embryos were selected to image single *col1a2*+ MPCs. Examples of centrally located MPCs (top panel) and MPCs along the VM (bottom panel) are shown. *col1a2*+ MPCs display ramified morphology with lamellipodia-like structures (arrows) and fine filopodia-like protrusions (arrowheads in expanded views). (D) *col1a2:Gal4; UAS:NTR-mCherry; UAS: Kaede* embryos were imaged at 2 dpf for 7.9 h. Stills from Movie 2 show the division of a *col1a2*+ MPC (arrows). Scale bars: 50 μm (C,D) and 20 μm (expanded views in D).

injured area, as indicated by the absence of *α-actin:GFP* expression at 1 hpi (hours post-injury), became substantially smaller at 24 hpi. This was accompanied by the emergence of elongated *mCherry*+ cells in the *GFP*‾ area, suggesting that *col1a2*+ cells were recruited to the injury site. By 48 hpi, the injury area was completely replaced by newly regenerated muscles, as indicated by higher level of *α-actin:GFP* expression compared with uninjured regions. At 72 hpi, on average 71% of the regenerated area was also labeled by *mCherry* expression (Fig. 4A; Fig. S4A), suggesting that *col1a2*+ cells contribute to newly formed fibers. Thus, needle injury experiments demonstrate that small muscle injuries in zebrafish can be quickly regenerated within 48 h, with potential contributions from *col1a2*+ MPCs.

We further investigated the expression kinetics of different markers during the entire process of muscle regeneration. Fish were injured by needle stabbing at 3 dpf and fixed at different time points (7, 24, 48, 76 hpi) for *in situ* analysis (Fig. 4B; Fig. S4B). The expression of MPC marker *pax7a* reached the highest level at the injury site at 24 hpi. The elevated *pax7a* expression remained at 48 hpi before returning to the basal level by 76 hpi. Analysis of several ECM genes (*col5a1*, *col1a2*, *col1a1a*, *cilp*, *postnb* and *sparc*) revealed similar expression kinetics as *pax7a* (Fig. 4B; Fig. S4B). By contrast, myogenic markers (*myoD* and *myogenin*) displayed kinetics slightly lagging behind *pax7a* and ECM markers. Their expression initiated at 24 hpi, peaked at 48 hpi, and returned to the basal level by 76 hpi. Double fluorescent *in situ* hybridization on injured embryos at 24 hpi revealed that high-level *col5a1* expression
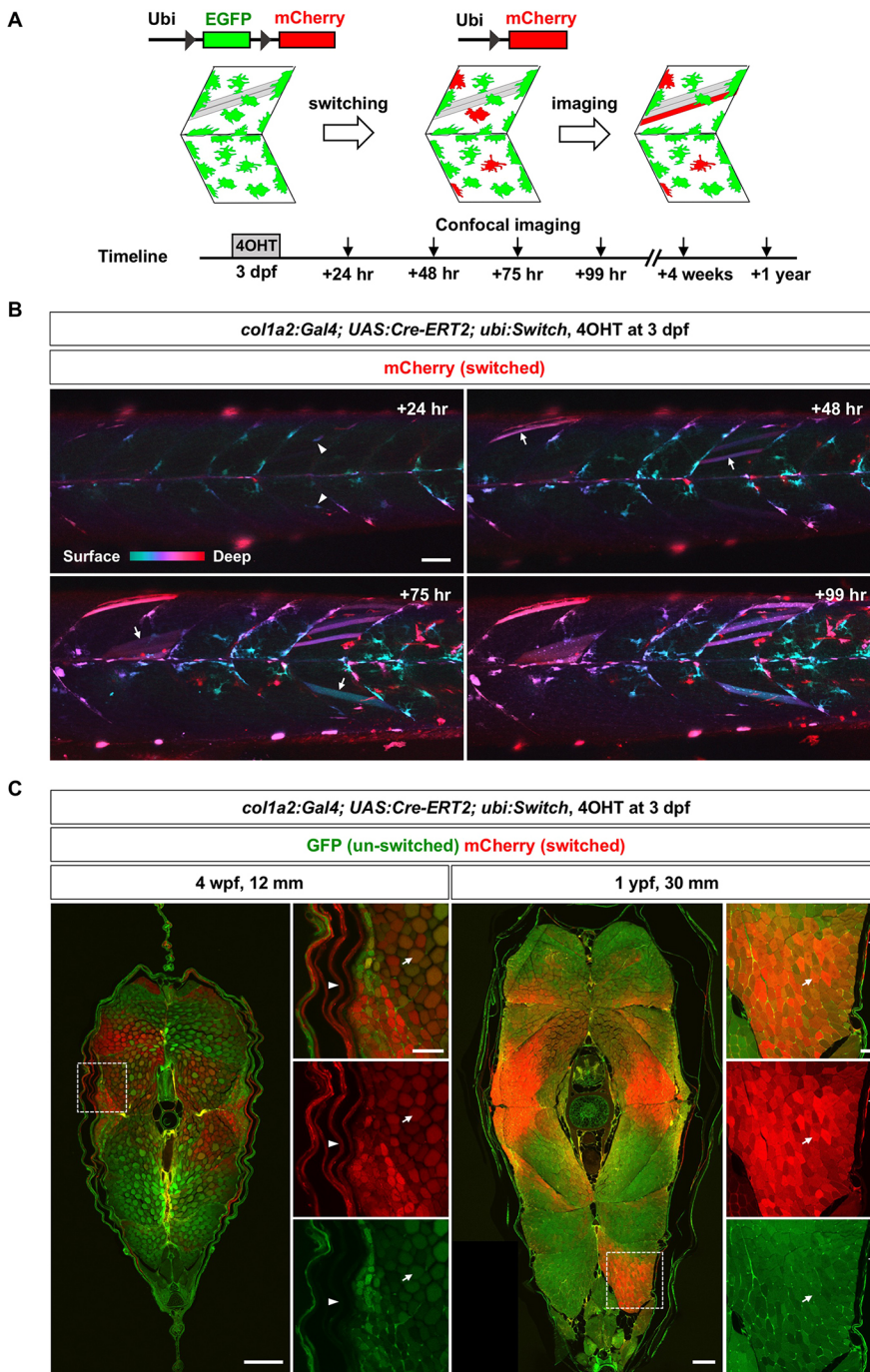
Fig. 3. *col1a2*^{+} cells contribute to muscle growth. (A) Schematics of Cre-mediated lineage tracing experiments. (B) *col1a2*[Cre-ERT2]; *ubi:Switch* embryos were pulsed with 4-OHT for 2 h at 3 dpf to induce EGFP excision, and imaged for 4 days. Color-coded depth projections of mCherry expression are shown. 'Switched' *mCherry*[+] MPCs (arrowheads) at the +24 h time point generated new *mCherry*[+] myofibers (arrows) starting from the +48 h time point. *n*=20 embryos. (C) 'Switched' *col1a2*[Cre-ERT2]; *ubi:Switch* fish were sectioned and imaged at 4 wpf (*n*=4 fish at 12 mm SL) and 1 ypf (*n*=4 fish at 30 mm SL). Transverse sections (stitched confocal tile scans) with expanded views of boxed regions are shown. Arrows denote *mCherry*[+] myofibers and arrowheads indicate the *mCherry*[+] skin. Scale bars: 50 μm (B,C) and 200 μm (full views in C).

at the injury site was accompanied by the elevated expression of *pax7a*, *myogenin* and *myoD* (Fig. 4C). Together, the time course of marker expression is consistent with the timing of muscle regeneration from the activation of MPCs to the differentiation of new myofibers (Fig. 4A). Our results suggest that *col1a2*[+] MPCs are not only recruited to the injury site to generate new myofibers, but also upregulate ECM gene expression perhaps to facilitate the regenerative process.

Single cell dynamics of *col1a2*[+] MPCs

We have shown that *col1a2*[+] MPCs contribute to new myofibers during both muscle growth and regeneration. To define the dynamic behavior of individual *col1a2*[+] MPCs *in vivo*, we performed single cell clonal analysis by taking advantage of the photoconvertible Kaede (Ando et al., 2002) and the mosaic nature of the *col1a2*[Kaede] line. Photoconversion of one isolated *Kaede*[green] MPC allowed us to visualize its cellular behavior and trace all of its *Kaede*[red] descendants. Briefly, we screened *col1a2*[Kaede] fish at 3 dpf and identified embryos with mosaic labeling of MPCs. Single isolated *Kaede*[green] cells were photoconverted with one cell per somite (1-4 cells per embryo) to ensure accurate cell tracing across multiple time points. We then used the 750 nm laser to introduce targeted muscle injury near one *Kaede*[red] cell. *Kaede*[red] MPCs in laser-ablated somites were designated as cells under 'injured' condition whereas photoconverted cells in uninjured somites were defined as 'control' cells. Individual embryos were imaged at 1, 24, 48 and 72 hpi to
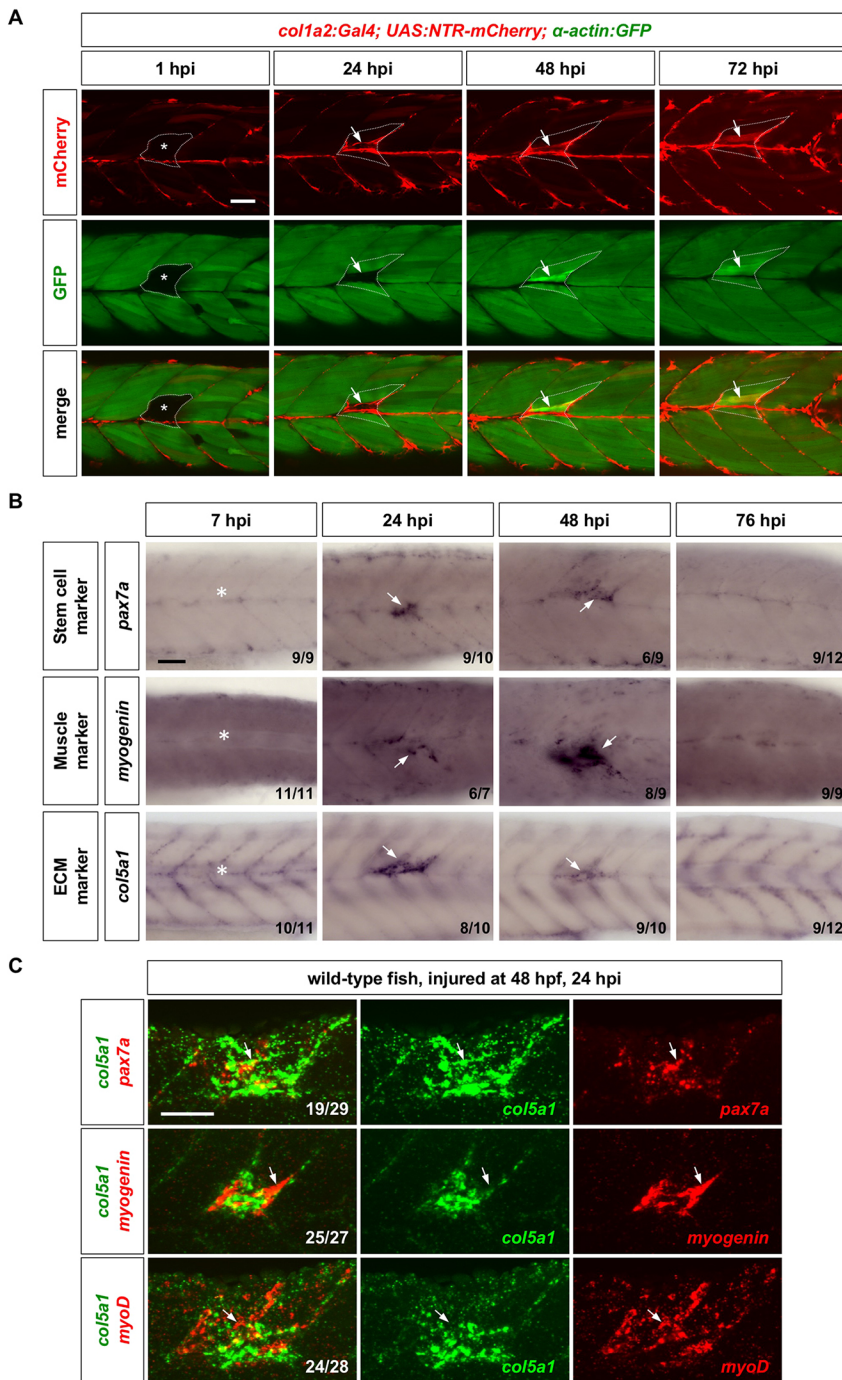
5

Fig. 4. ECM dynamics during muscle regeneration. (A) *col1a2^NTR-mCherry*; *α-actin:GFP* embryos were needle injured at 3 dpf, and imaged at 1, 24, 48 and 72 hpi. Injured muscles (asterisks) can be identified by the lack of *α-actin:GFP* expression (green) at 1 hpi, whereas regenerated muscles are marked by slightly elevated *α-actin:GFP* expression. *mCherry^+* cells (arrows) emerged at the site of injury at 24 hpi, and generated new *mCherry^+* myofibers by 72 hpi. Dotted lines outline the injured/regenerated regions. *n*=17 embryos. (B) Wild-type embryos were needle stabbed to injure muscles near the end of yolk extension (asterisks) at 3 dpf and stained for several markers (*pax7a*, *myogenin* and *col5a1*) at different time points. (C) Muscles of wild-type embryos were injured by needle stabbing at 48 hpf and double stained at 24 hpi using the *col5a1* probe (green) with either *pax7a*, *myogenin* or *myoD* probes (red, arrows). Representative images are shown with the *n* number indicated for each staining in B and C. Scale bars: 50 μm.

capture the behaviors of individual *Kaede^red* MPCs and their descendants (Fig. 5A). Since we found that *col1a2^+* MPCs along the HM rarely divide (as shown previously by Nguyen et al., 2017), we focused our analysis on centrally located and VM-associated MPCs. Together, we followed 133 *col1a2^+* MPCs in 56 embryos.

Based on cell behaviors of each clone, we categorized the response of *col1a2^+* MPCs into four different groups (Fig. 5B). In the type I response, cells did not proliferate and maintained the ramified morphology throughout 72 h. In the type II response, cells underwent one or more cell divisions, but all daughters maintained the ramified morphology, suggesting a quiescent state. By contrast, in the type III response, cells generated small elongated cells, which were usually bi-polar with processes extending along myofibers.

This is markedly distinct from the multipolar ramified morphology of quiescent *col1a2^+* MPCs, suggesting an activated state. Lastly, in the type IV response, cells first gave rise to small elongated cells similar to those in the type III response, some of which later generated one or more *Kaede^red* myofibers by 72 hpi. As Kaede protein appeared to concentrate in the nuclei of muscle cells (Fig. S5A,B), new myofibers generated from *Kaede^red* cells can be easily identified based on the stronger *Kaede^red* signal in the oval-shaped nucleus with a weaker and diffusive signal in the cytoplasm spanning the width of a somite. Antibody staining revealed that the *Kaede^+* nucleus of a newly generated muscle no longer expressed Pax7 (a feature typical of differentiated muscles), whereas small elongated cells in between myofibers remained *Pax7^+* (Fig. S5C).
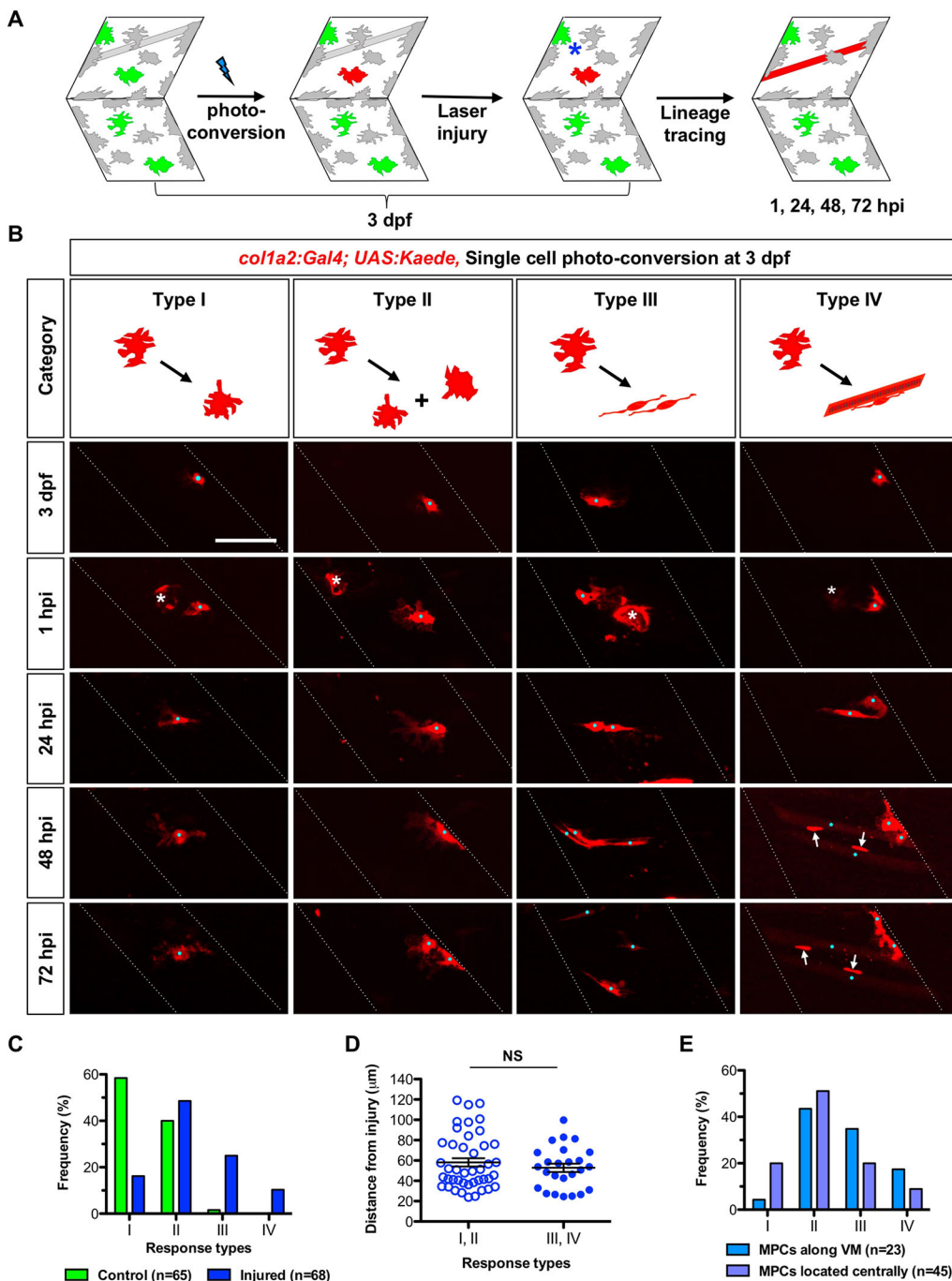
Fig. 5. Single cell clonal analysis of *col1a2*+ MPCs. (A) Schematics of single cell lineage tracing. Isolated *Kaede*^{green} MPCs in *col1a2*^{Kaede} fish at 3 dpf were photoconverted to *Kaede*^{red}. Immediately after the photoconversion, muscles near the *Kaede*^{red} cell were damaged by laser ablation (asterisk). The lineage of the *Kaede*^{red} cell was inferred by imaging the same region every 24 h. (B) Single cell lineage tracing in *col1a2*^{Kaede} embryos. Four types of responses are represented in cartoons on top with corresponding examples shown at the bottom. Each embryo was imaged at 3 dpf immediately after the photoconversion but before the injury and then at 1, 24, 48, 72 hpi. Note that laser ablation often resulted in elevated autofluorescence at the center of the injury (asterisks). Individual *col1a2*+ MPCs and their descendants are marked with cyan dots. The nuclei of newly formed myofibers can be identified by high level of *Kaede*^{red} expression (arrows). (C) Quantification of response types of *col1a2*+ MPCs. (D) Quantification of cell distance from the injury site in different response types. Each point represents one *col1a2*+ MPC under injured conditions (n=68 cells). Type I/II (empty dots) and III/IV (solid dots) responses represent quiescent and activated cells, respectively. Data are plotted as mean±s.e.m. Statistics: Mann–Whitney *U*-test. NS, not significant. (E) Quantification of response types of *col1a2*+ MPCs with respect to their initial locations. MPCs along the VM (n=23) are more likely to generate type III/IV responses compared with centrally located MPCs (n=45). Scale bar: 50 μm.

Together, under uninjured conditions, *col1a2*+ MPCs generated predominantly type I (58%, 38/65 cells) or type II (40%, 26/65 cells) responses, but rarely type III response (2%, 1/65 cells) and never a type IV response (Fig. 5C). By contrast, cells under injured conditions exhibited all four types of responses, with a combined 35% (24/68 cells) in the type III and IV categories. Similarly, 24% (16/68 cells) of *col1a2*+ MPCs in injured conditions generated clones of at least 3 cells compared with only 2% (1/65 cells) in control conditions (Fig. S5D), suggesting an increase in cell proliferation during muscle regeneration. These results suggest that type III/IV behaviors represent the muscle regenerative response of activated *col1a2*+ MPCs. Since the formation of new myofibers was always preceded by small elongated cells (Fig. 5B), the type III

response likely represents a transitional phase before the type IV response.

Since not all *col1a2*+ MPCs would respond to the injury in the same somite (Fig. 5B,C), we asked whether the initial position of the cell influences its behavior. We found that the distance from the injury to the center of the labeled MPCs did not correlate with the type of response (Fig. 5D). For example, some cells 24 μm away failed to respond to the injury whereas other cells >80 μm away became activated. This result suggests that *col1a2*+ MPCs can detect and respond to an injury at a long distance away from the cell body. Interestingly, *col1a2*+ MPCs located along the VM were slightly more likely to generate a type III or IV response (52%, 12/23 cells) than centrally located cells (29%, 13/45 cells) (Fig. 5E),

suggesting that the local niche might influence the behavior of MPCs or that there are multiple types of MPCs that differentially respond to injury.

New myofibers are predominantly generated by cell fusion

Our single cell clonal analysis reveals that activated $col1a2^+$ MPCs go through a series of stereotypic phases to generate new myofibers. To further test this, we carried out confocal time-lapse imaging to visualize the entire process of muscle regeneration. First, we imaged the 'early phase' of muscle regeneration at 0-23 hpi (Fig. 6A). Mosaic $col1a2^{Kaede}$ embryos were injured by needle stabbing at 59 hpf. Individual $Kaede^{green}$ MPCs were photoconverted to facilitate cell tracking (Fig. 6B; Movie 3). Within the first few

hours, the activated $col1a2^+$ MPC started to project polarized cellular processes along myofibers. This bi-polar and elongated morphology was maintained even after cell division. Consistent with our clonal analysis, new myofibers were never generated during this time interval. Thus, the early phase of muscle regeneration is characterized by the morphological changes and proliferations of activated $col1a2^+$ MPCs.

Next, we imaged the 'late phase' of muscle regeneration in mosaic $col1a2^{Kaede}$ embryos at 29-48 hpi (Fig. 6C). Remarkably, all new myofibers formed in a similar manner: a small elongated $Kaede^+$ MPC visible at one time point disappeared by the next time point (8-min intervals), with simultaneous emergence of $Kaede^+$ myofiber characterized by $Kaede^{strong}$ nucleus and $Kaede^{weak}$
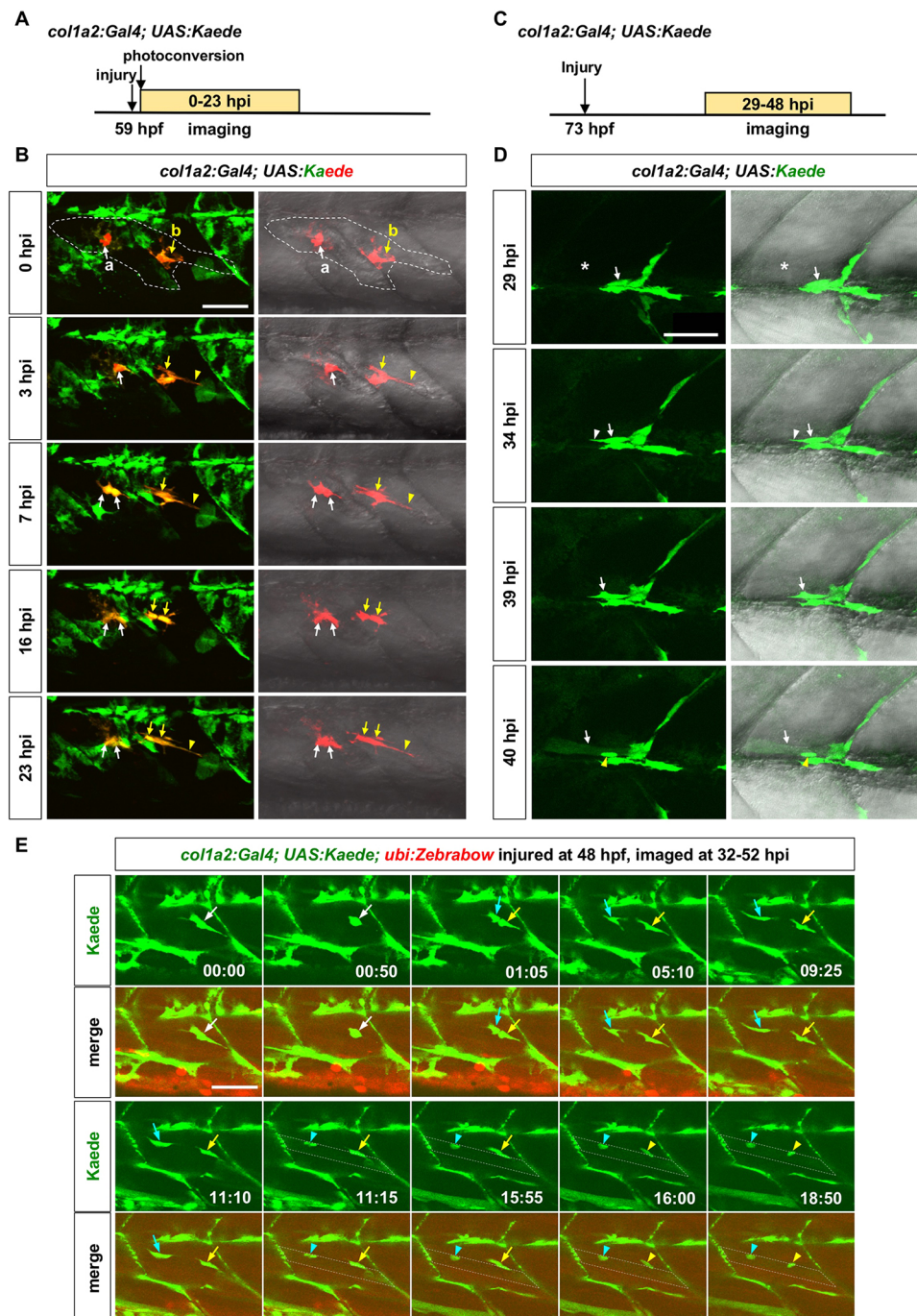

Fig. 6. *In vivo* dynamics of $col1a2^+$ MPCs during muscle regeneration. (A) Experimental design. $col1a2^{Kaede}$ embryos were needle injured, photoconverted at 59 hpf, and imaged at 0-23 hpi. (B) Still images from Movie 3 show the dynamics of 2 $Kaede^{red}$ cells. Both cells were within the muscle injury area (outlined by dashed lines). Cell labeled 'a' (white arrows) maintained the ramified morphology, and divided once at 7 hpi generating two daughter cells with similar morphologies. By contrast, cell 'b' (yellow arrows) extended to form an elongated morphology (arrowheads), and divided once at 16 hpi generating two polarized daughter cells. n=6 embryos. (C) Experimental design. Mosaic $col1a2^{Kaede}$ embryos were injured at 73 hpf, and imaged at 29-48 hpi. (D) Stills from Movie 4 show that a $Kaede^+$ MPC (arrows) near the injury site (asterisks) elongated at 34 hpi (white arrowheads), formed protrusions at 39 hpi, and fused with a neighboring myofiber at 40 hpi. The new myofiber can be visualized by the weak Kaede expression throughout the muscle cytoplasm and the strong Kaede signal in the nucleus (yellow arrowheads). n=13 fusion events from 9 embryos. (E) $col1a2^{Kaede}$; ubi: Zebrabow embryos were injured at 48 hpf and imaged at 32-52 hpi. Stills from Movie 6 are shown with time stamps (hh:mm) indicated. A $Kaede^+$ MPC (white arrows) divided between 00:50 and 01:05. The anterior daughter (cyan arrows) fused with a myofiber (dotted lines) between 11:10 and 11:15, while the posterior daughter (yellow arrows) fused with the same myofiber between 15:55 and 16:00. Concentrated Kaede expression in the nucleus after the cell fusion was clearly visible (arrowheads of corresponding colors). n=31 fusion events from 12 embryos, of which 3 pairs of sibling cells sequentially fused with the same myofiber, as shown in E. Scale bars: 50 µm.

cytoplasm (Fig. 6D; Movie 4). The rapidity of this event suggests that new myofibers are formed through cell fusions between a $Kaede^+$ MPC and an existing non-labeled myofiber. To test this model further, we performed time-lapse imaging on $col1a2^{NTR-mCherry}$; α-actin:GFP embryos. Similar cytoplasmic spread of the mCherry signal was observed after the fusion of an $mCherry^+$ MPC with a neighboring GFP^+ myofiber (Movie 5).

To better characterize the behavior of $col1a2^+$ MPCs, we performed similar cell tracking experiments at high temporal resolution (5-min intervals) using $col1a2^{Kaede}$; $ubi:Zebrabow$ embryos. Nuclear localization of the Kaede protein in myofibers allowed us to track the nucleus even after the cell fusion. $ubi:Zebrabow$ was used to visualize myofibers as it was expressed strongly in muscles but at a very low level in $col1a2^+$ MPCs. We observed a total of 31 fusion events from 12 embryos, all of which displayed similar kinetics to those described above (Fig. 6E; Fig. S6; Movie 6). The disappearance of cell processes was accompanied by simultaneous spreading of the Kaede signal in the cytoplasm of an RFP^+ myofiber. Of all fusion events, we identified 3 pairs of $Kaede^+$ sibling cells from 3 different embryos. Intriguingly, in all 3 cases, the two sibling cells fused sequentially to the same muscle, resulting in the addition of two new nuclei to one existing myofiber. This result suggests that sequential fusion of sibling MPCs is one mechanism to grow existing myofibers to replace injured muscles.

Increased frequency of de novo fiber formation during muscle regeneration

Since we never observed any *de novo* fiber formation in our time-lapse movies, we asked whether muscles are formed exclusively through cell fusions. To answer this question, we performed Cre-mediated lineage tracing in $col1a2^{Cre-ERT2}$; $ubi:Switch$ fish (Fig. 7A). Embryos at 3 dpf were pulsed with 4-OHT for 3.5 h to mosaicly label $col1a2^+$ MPCs. Fish were then injured by needle stabbing and imaged at 75 hpi to quantify newly formed $mCherry^+$ myofibers. Since only a small fraction of $col1a2^+$ MPCs were switched and labeled by mCherry, there are three possible modes of generating a new myofiber (Fig. 7B): (1) fusion of an $mCherry^+$ MPC with an existing $EGFP^+$ myofiber (MPC-muscle fusion); (2) fusion of an $mCherry^+$ MPC with one or more $EGFP^+$ MPCs (MPC-MPC fusion); and (3) *de novo* formation of a nascent fiber from an $mCherry^+$ MPC. The first two cases (cell fusions) would result in an $EGFP^+mCherry^+$ myofiber, while the third scenario (*de novo* formation) would result in an $EGFP^-mCherry^+$ myofiber. In uninjured controls, 97% of new myofibers (37/38) were formed via cell fusion, whereas only 3% of fibers (1/38) were generated *de novo* (Fig. 7C,D). Interestingly, in injured embryos, *de novo* fiber formation increased about 5-fold to 14% (14/98) at the muscle injury site. Combined with our time-lapse imaging data, this result suggests that during larval growth, new myofibers are generated predominantly through fusion of $col1a2^+$ MPC descendants with existing myofibers; however, under injury conditions, more muscles are regenerated through *de novo* fiber formation.

col1a2+ MPCs are required for effective muscle regeneration

To test whether $col1a2^+$ MPCs are essential for embryonic muscle regeneration, we partially ablated $col1a2^+$ cells using a nitroreductase (NTR)-based system. The NTR enzyme converts the harmless prodrug metronidazole (MTZ) into a cytotoxic compound that induces rapid cell death of NTR-expressing cells (Curado et al., 2008; Pisharath et al., 2007). We selected $col1a2^{NTR-mCherry}$ embryos with a modest expression level to avoid high perduring NTR-mCherry expression in muscles. Compared with

water-treated controls, MTZ-treated $col1a2^{NTR-mCherry}$ embryos showed a 59% reduction in the number of $Pax7^+$ cells, including both superficial MPCs and deep fiber-associated MPCs (Fig. 7E,F). We then analyzed muscle regeneration in embryos with partially depleted $col1a2^+$ MPCs. $mCherry^+$ embryos and $mCherry^-$ controls from a $col1a2^{NTR-mCherry}$ outcross were treated with MTZ at 2-3 dpf, injured at 3 dpf and fixed at 24 hpi for *in situ* analysis. Similarly to our previous observations (Fig. 4; Fig. S4B), most $mCherry^-$ controls showed substantial upregulation of both *myogenin* and *myoD* at the injury site at 24 hpi (Fig. 7G). By contrast, the majority of ablated embryos showed no or only modest upregulation of myogenic markers at the injury site, suggesting a compromised regenerative response. This result suggests that $col1a2^+$ MPCs are required for efficient regeneration of muscle injury in zebrafish embryos.

DISCUSSION

Our study provides a dynamic view of embryonic MPCs in the zebrafish dermomyotome during muscle growth and regeneration. First, $col1a2^+$ MPCs display a unique ramified morphology and express many ECM genes. Second, lineage tracing experiments show that $col1a2^+$ MPCs contribute to normal muscle growth as well as muscle regeneration. Third, $col1a2^+$ MPCs undergo a series of stereotypical steps to generate new muscle fibers, predominantly by cell fusions with existing myofibers.

col1a2+ MPCs in zebrafish are functionally equivalent to the amniote dermomyotome

Dermomyotome is an evolutionarily conserved structure on the external surface of the myotome present in most vertebrates (Devoto et al., 2006). Using a novel $col1a2$ transgenic line, we identified a population of $col1a2^+$ cells on the surface of the somite that co-expresses the MPC marker Pax7. The location, distribution and marker expression of $col1a2^+$ MPCs are consistent with what has been described as the dermomyotome, or the external cell layer, in zebrafish (Devoto et al., 2006; Feng et al., 2006; Hammond et al., 2007). Previous work in mouse and chick has shown that satellite cells originate from the embryonic dermomyotome (Gros et al., 2005; Kassar-Duchossoy et al., 2005; Relaix et al., 2005; Schienda et al., 2006). Similarly, using lineage tracing and time-lapse imaging, we showed that $col1a2^+$ MPCs contribute not only to new myofibers but also to small $Pax7^+$ fiber-associated cells, which likely correspond to larval MPCs (Gurevich et al., 2016; Nguyen et al., 2017; Pipalia et al., 2016; Roy et al., 2017; Seger et al., 2011). In amniotes, the dermomyotome has also been shown to give rise to the dermis (Christ and Scaal, 2008; Stellabotte and Devoto, 2007). However, previous short-term cell tracing experiments with dye labeling in zebrafish have not reached an agreement on whether the anterior somitic compartment (precursors of the dermomyotome) contributes to the dermis (Hollway et al., 2007; Stellabotte et al., 2007). Using Cre-mediated lineage tracing, we found that although short-term lineage tracing of $col1a2^+$ MPCs (3 days) showed no contribution to the skin, long-term tracing for more than a month revealed substantial labeling of the skin. Our finding is consistent with a previous report that the zebrafish dermis is acellular during the first 3-4 weeks of development (Le Guellec et al., 2004). Together, our results suggest that $col1a2^+$ MPCs are functionally equivalent to the amniote dermomyotome, contributing to both the dermis and muscles. Several scenarios might explain our observations. First, superficial $col1a2^+$ cells on the somite at 3 dpf might be bi-potential and thus capable of generating both dermal and muscle lineages. Second, these superficial $col1a2^+$ cells
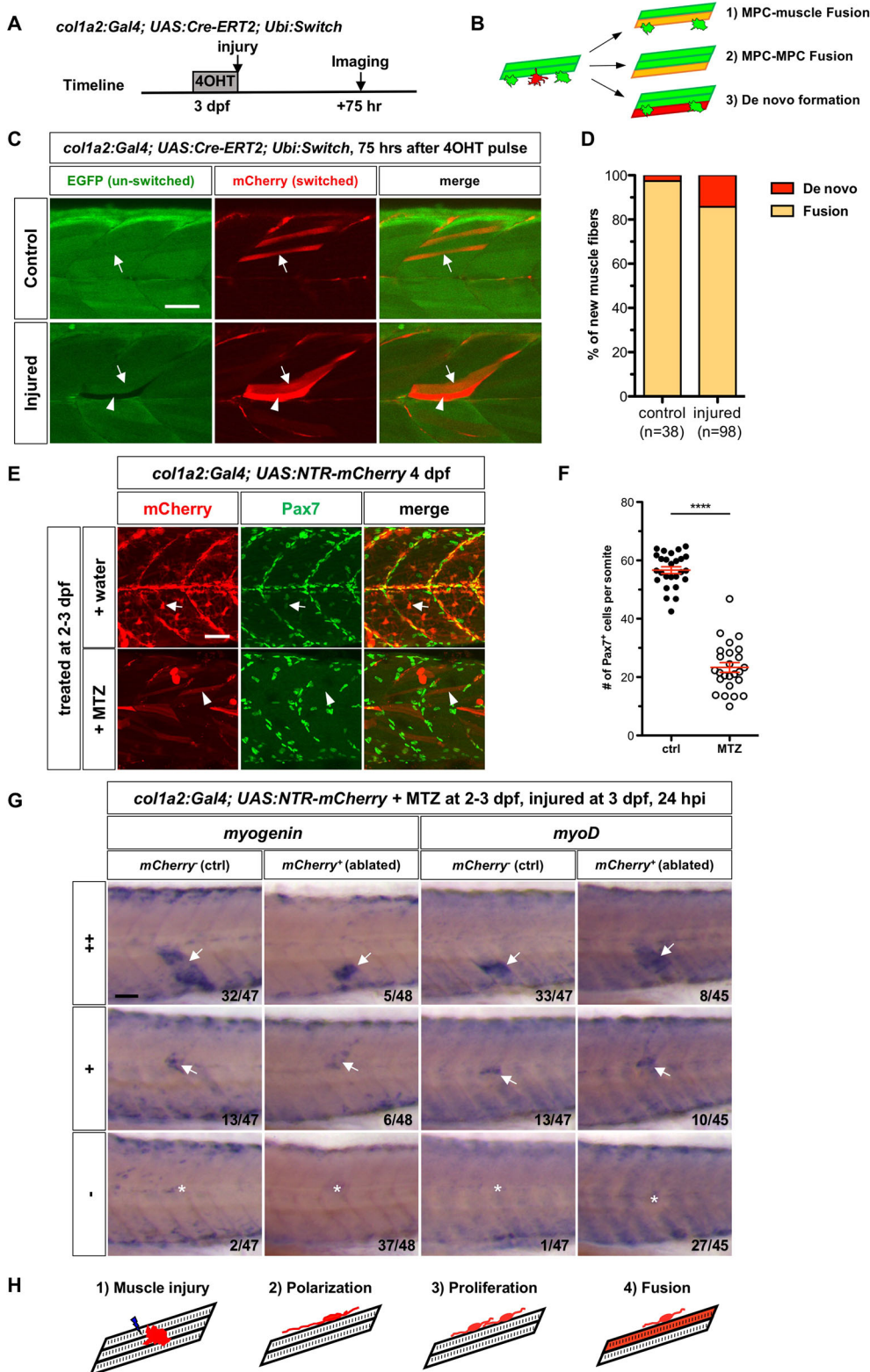
Fig. 7. col1a2+ MPCs generate new myofibers primarily by cell fusion.
(A) Experimental design. col1a2$^{Cre-ERT2}$; ubi:Switch embryos treated with 4-OHT for 3.5 h at 3 dpf were either needle injured or left uninjured (controls) and imaged 75 h later. (B) Three possible modes of new myofiber formation. (C) In controls (n=20), new myofibers were formed primarily through cell fusion (arrows), whereas in injured embryos (n=19), new fibers were generated by both fusion (arrows) and occasionally, de novo fiber formation (arrowheads). (D) Quantification of modes of new myofiber formation. The number of new myofibers scored is shown. (E) col1a2$^{NTR-mCherry}$ embryos treated with either water or MTZ at 2-3 dpf were stained with the mCherry (red) and the Pax7 (green) antibodies at 4 dpf. Water-treated controls showed many mCherry+Pax7+ MPCs (arrows), whereas MTZ-treated embryos lost most mCherry+ MPCs with a few spared myofibers (arrowheads). (F) Quantification of the average number of Pax7+ MPCs per somite, including superficial MPCs and deep myofiber-associated MPCs shown in E. n=26 (control) and 25 (MTZ). Data are plotted as mean±s.e.m. Statistics: Mann–Whitney U-test. ****P<0.0001. (G) col1a2$^{NTR-mCherry}$ embryos (ablated) or mCherry^{-} siblings (control) were treated with MTZ at 2-3 dpf, injured at 3 dpf and stained for myogenin or myoD expression at 24 hpi. Embryos were scored based on the extent of expression of myogenic markers at the injury site: high level (++), mid-level (+) and no induction (−). The number of embryos in each category is indicated. Arrows denote induced marker expression and asterisks indicate the injury site in the case of no induction. (H) Model of muscle regeneration by col1a2+ MPCs. Scale bars: 50 µm.

might be heterogeneous, containing distinct dermal progenitors and muscle progenitors. Lastly, in an unlikely scenario, col1a2+ cells deep around the notochord could contribute to dermal progenitors that migrate mediolaterally through muscles and populate the dermis at 4 wpf. Future experiments on single cell lineage analysis will help distinguish the first two more likely possibilities.

Using the same col1a2 reporter, we found that the superficial layer of col1a2+ cells immediately adjacent to muscles persists in adult zebrafish, likely corresponding to the presumptive dermomyotome described previously (Hollway et al., 2007). This observation is in contrast with the situation in the amniote dermomyotome, which is a transient embryonic structure (Christ and Scaal, 2008; Stellabotte and

DEVELOPMENT

10

Devoto, 2007). The persistence of the dermomyotome in adult zebrafish provides another source of MPCs in addition to satellite-like cells (Berberoglu et al., 2017) for the continuous growth of the fish.

Unique features of *col1a2*[+] MPCs

Using *col1a2* transgenic lines, we discovered some unique features of *col1a2*[+] MPCs. First, *col1a2*[+] MPCs display a ramified morphology with dynamic cellular processes. In the quiescent state, these cells are not polarized, showing lamellipodia-like structures all around the cell. This morphology contrasts with that of mouse satellite cells, which usually display a bipolar morphology with short processes extending along the myofiber (Webster et al., 2016). Although cell bodies of *col1a2*[+] MPCs are mostly stationary in uninjured conditions, their cellular processes are quite dynamic, constantly extending and retracting. Each cell and its processes occupy a largely non-overlapping area, reminiscent of the tiling of neuronal dendrites (Grueber and Sagasti, 2010). During cell divisions, the mother cell retracts all its processes, but immediately after the division, the two daughter cells would extend new processes to reclaim the similar surface area. These dynamic behaviors might ensure the complete coverage of the somitic surface and detect potential muscle injuries. Moreover, we often observed long filopodia-like structures extending from *col1a2*[+] MPCs. Intriguingly, our single cell clonal analysis revealed that the distance between the cell body of a *col1a2*[+] MPC and the injury site is not a reliable predictor of whether the MPC would generate a regenerative response. It thus raises the possibility that the long cellular projections might allow *col1a2*[+] MPCs to detect muscle injury at a significant distance from the cell body. Interestingly, dermomyotome cells in chick display similar filopodia-like protrusions, facilitating the interaction with the overlying ectoderm during somite development (Sagar et al., 2015).

Second, we found that embryonic MPCs in the dermomyotome express a number of ECM genes, including *col1a2*, *col5a1* and *cilp*. Similarly, *col1a1* and *cilp* are expressed in what is described as a dermomyotome-like domain in trout embryos (Ralliere et al., 2015; Rescan et al., 2005). Moreover, we found that the expression of these ECM genes is dynamically induced during muscle regeneration. Our observations in embryonic MPCs in zebrafish show strong similarities to gene expression in mouse MPCs. For example, fetal muscle stem cells in mice show high-level expression of several ECM molecules, such as tenascin-C (*TnC*), fibronectin (*Fn1*) and collagen VI (*Col6*) (Tierney et al., 2016). Similarly, recently identified *Twist2*^{+} MPCs in mouse show enrichment of many ECM genes, including *Col1a1*, *Col1a2* and *Cilp* (Liu et al., 2017). Interestingly, although quiescent adult satellite cells do not express high levels of ECM genes (Liu et al., 2017), activated satellite cells show upregulation of many collagen genes, such as *Col1a1* and *Col1a2* (Pallafacchina et al., 2010). Thus, dynamic regulation of ECM gene expression might be a common feature of MPCs.

Does the ECM play an active role in regulating the function of MPCs? We envision two non-mutually exclusive scenarios. First, the ECM might be an integral part of the niche that maintains the self-renewing property of MPCs. Recent work has implicated many ECM components, including fibronectin, tenascin-C, laminins and collagens, as critical niche factors that modulate satellite cell function (Bentzinger et al., 2013b; Fry et al., 2017; Rayagiri et al., 2018; Tierney et al., 2016; Urciuolo et al., 2013). In particular, it has been shown that collagen V produced by adult muscle satellite cells is an essential component of the quiescent niche, as deletion of the *Col5a1* gene results in depletion of the stem cell pool (Baghdadi et al., 2018). The close association of most *col1a2*[+] MPCs with the

ECM-rich myoseptum (Charvet et al., 2011) suggests that the myoseptum might function as the niche for embryonic MPCs in zebrafish. Second, the induction of ECM gene expression upon muscle injury might provide the appropriate scaffold for the recruitment and/or migration of activated MPCs. Consistent with this idea, intravital imaging of muscle regeneration in mice reveals that ECM remnants from injured myofibers provide cues to regulate satellite cell behavior (Webster et al., 2016). Future studies will need to determine whether loss of any ECM component would compromise the regenerative capacity of *col1a2*[+] MPCs in zebrafish.

col1a2[+] MPCs contribute to muscle growth and regeneration

Previous studies using different *pax7* reporter lines have led to different conclusions on the role of MPCs during muscle regeneration. For example, it has been shown that *pax7a*[+] MPCs do not participate in regenerating a small focal muscle injury, although they do contribute to new myofibers during the regeneration of a large injury (Knappe et al., 2015). This observation is in contrast with the work by Pipalia et al., which has shown that both *pax7a*[+]*pax7b*[−] and *pax7b*[+] MPCs contribute to new myofibers during muscle regeneration (Pipalia et al., 2016). These studies rely on GFP perdurance in new myofibers to infer that they originate from *GFP*[+] MPCs. Differences in GFP stability in different transgenic lines could complicate lineage interpretations. To definitively address this issue, we performed Cre-mediated lineage tracing of *col1a2*[+] MPCs. We demonstrated that *col1a2*[+] MPCs not only contribute to new myofibers during normal larval development but also generate new muscles during regeneration of small injuries. Long-term tracing of descendants of embryonic *col1a2*[+] MPCs revealed substantial contribution to adult muscles, suggesting that *col1a2*[+] MPCs also give rise to larval/adult MPCs to sustain the growth of skeletal muscles.

Another question that needs to be clarified is the functional requirement of different MPC populations during muscle regeneration. Pipalia et al. have shown that muscle regeneration occurs normally despite the ablation of *pax7b*[+] MPCs, which include superficial MPCs in the dermomyotome and deep fiber-associated MPCs (Pipalia et al., 2016). By contrast, depletion of a small subset of deep myotomal cells co-labeled by *cmet* and *pax7a* results in a failure to initiate regeneration (Gurevich et al., 2016). Although the lineage relationship between *pax7b*[+] and *cmet*[+] MPCs remains to be established, it raises the question which population of MPCs is essential for muscle regeneration. In our studies, partial depletion of *col1a2*[+] MPCs resulted in significantly blunted regenerative response. Since *col1a2*[+] MPCs are likely to include both *pax7a*[+] and *pax7b*[+] progenitors, one parsimonious explanation is that *pax7a*[+] MPCs might play a more prominent role in mounting the regenerative response.

Our newly developed *col1a2:Gal4* transgenic line provides a useful alternative to existing *pax7*-based transgenes in studying the dynamics of embryonic MPCs. By taking advantage of the variegated nature of the *col1a2*[Kaede] line and the photoconvertible Kaede, we performed single cell clonal analysis of *col1a2*[+] MPCs. A quiescent *col1a2*[+] MPC (type I/II responses) maintains its ramified morphology even after occasional cell divisions. By contrast, an activated *col1a2*[+] MPC (type III/IV responses) undergoes several stereotypic steps to generate new myofibers (Fig. 7H). First, it changes from its resting ramified morphology to an elongated and polarized morphology, usually within the first 3-5 h after injury. The cell extends long cellular projections along the longitudinal axis of neighboring myofibers. Next, the activated MPC undergoes several rounds of cell divisions generating a clone

of small polarized daughter cells by 12-24 hpi. Finally, by 72 hpi, new myofibers emerge at the injury site, predominantly formed through fusions between descendants of *col1a2*[+] MPCs and existing myofibers (discussed below). The dynamic behaviors of an activated *col1a2*[+] MPC, such as the initial polarization phase, are reminiscent of *myf5*[+] fiber-associated MPCs during muscle regeneration (Gurevich et al., 2016). However, unlike *myf5*[+] MPCs, *col1a2*[+] MPCs never cross the myoseptum to regenerate muscle injury in neighboring somites. Quantification of the clonal analysis further revealed that although the distance to the injury did not enable us to predict the cellular responsiveness, *col1a2*[+] MPCs located along the VM were slightly more likely to respond to the injury than centrally located MPCs. One explanation is that VM-associated MPCs are better equipped to sense and respond to injury with slightly longer filopodia compared to central MPCs. Alternatively, the ECM-enriched myoseptum might provide the scaffold to facilitate the migration of activated *col1a2*[+] MPCs.

col1a2[+] MPCs generate new myofibers predominantly by cell fusion

Two independent lines of evidence indicate that *col1a2*[+] MPCs generate new myofibers primarily through cell fusion. First, time-lapse imaging of the regeneration process at high temporal resolution in different *col1a2* reporter lines showed that the emergence of a new *Kaede*[+] or *mCherry*[+] myofiber always appeared to be completed between two time points (5- to 8-min intervals), accompanied by the simultaneous disappearance of the *col1a2*[+] MPC. The absence of intermediate steps, such as searching for attachment sites along the myoseptum, suggests that new myofibers are formed by cell fusion rather than *de novo* fiber formation. Consistent with this result, our Cre-mediated lineage tracing experiments showed that most new myofibers expressed both EGFP and mCherry, suggesting that cell fusion events between a 'switched' *mCherry*[+] MPC and an 'un-switched' *EGFP*[+] myofiber occurred. Indeed, long-term tracing of *col1a2*[+] MPCs showed that almost all *mCherry*[+] myofibers were also *EGFP*[+], suggesting that fusion is also the predominant mode of muscle growth in adult zebrafish. Intriguingly, during muscle regeneration, a 5-fold increase in *de novo* fiber formation (14%) was observed compared with uninjured conditions (3%). This result suggests that *de novo* fiber formation is specifically induced during muscle regeneration to combat the increasing demand to replace damaged fibers. This might be achieved by differential activation of sub-populations of *col1a2*[+] MPCs. Pipalia et al. (2016) have previously shown that *pax7b*[+] MPCs contribute to muscle growth and regeneration by cell fusions, whereas *pax7a*[+]*pax7b*[−] MPCs predominantly generate nascent fibers. Considering our findings, one possibility is that normal muscle growth is primarily contributed by *pax7b*[+] MPCs, whereas muscle injury activates both *pax7b*[+] and *pax7a*[+]*pax7b*[−] MPCs.

In summary, our work provides a dynamic view of *col1a2*[+] MPCs during muscle growth and regeneration. It also raises additional questions for future investigations. For example, what is the injury signal that activates *col1a2*[+] MPCs? Tissue injury is often associated with an elevated level of reactive oxygen species (ROS) and the recruitment of patrolling immune cells such as macrophages and neutrophils (Love et al., 2013; Niethammer et al., 2009). It is therefore plausible that ROS and/or cytokines secreted by immune cells might be the trigger to activate MPCs. Indeed, mouse and human data have implicated macrophages and other immune cells as the critical regulators of satellite cell functions (Bentzinger et al., 2013a; Saclier et al., 2013).

MATERIALS AND METHODS

Zebrafish strains

Zebrafish strains were maintained and raised according to standard protocols (Westerfield, 2000). All animal research was conducted in accordance with the principles outlined in the current Guidelines of the Canadian Council on Animal Care. All protocols were approved by the Animal Care Committee at the University of Calgary (#AC17-0128). Embryos were grown at 28.5°C and staged as previously described (Kimmel et al., 1995). Fish older than 24 hpf were treated with 1-phenyl 2-thiourea (PTU) to prevent pigmentation. TL and TL/AB wild-type strains were used in this study along with the following transgenic lines: *α-actin:GFP* (Higashijima et al., 1997), *col1a2:Gal4* (Ma et al., 2018), *ptc2:Kaede* (Huang et al., 2012), *UAS:Kaede* (Scott et al., 2007), *UAS:NTR-mCherry* (Davison et al., 2007), *UAS:Cre-ERT2*, *ubi:loxP-EGFP-loxP-mCherry* (*ubi:Switch*) (Mosimann et al., 2011), and *ubi:Zebrabow* (Pan et al., 2013). The mosaic *col1a2:Gal4; UAS:Kaede* line was maintained by selectively growing embryos with more mosaic Kaede expression.

Generation of transgenic lines

UAS:Cre-ERT2 transgenic fish were generated by standard Tol2-mediated transgenesis (Suster et al., 2009). To generate *col1a2:Gal4* transgenic line, BAC (bacteria artificial chromosome) clone zC122K13 from the CHORI-211 library that contains *col1a2* genomic region with 78 kb upstream and 58 kb downstream regulatory sequences was selected for bacteria-mediated homologous recombination following the standard protocol (Bussmann and Schulte-Merker, 2011). Briefly, the pRedET plasmid was first transformed into BAC-containing bacteria. Second, an iTol2_amp cassette containing two Tol2 arms in opposite directions flanking an ampicillin resistance gene was recombined into the vector backbone of zC122K13. Lastly, a cassette containing the Gal4-VP16 with a kanamycin-resistant gene was recombined into zC122K13-iTol2_amp to replace the first coding exon of the *col1a2* gene. After each round of recombination, successful recombinants were confirmed by PCR analysis. The final *col1a2:Gal4* BAC was then co-injected with *tol2* transposase mRNA into *UAS:Kaede* embryos at one-cell stage. Positive transgenic lines were identified by screening Kaede expression in F1 embryos from injected founders.

Muscle injury

Two methods were employed to generate small focal muscle injury at specific locations in larval zebrafish. In needle injury, we used a sharp injection needle to stab muscles near the end of yolk extension (somites 17-19) so the injury site could be located easily during the lineage tracing. Alternatively, to introduce muscle injury at a more precise location, laser ablation was performed with the 750 nm laser and 25× objective on the Leica TCS SP8 multi-photon microscope. A region of interest (ROI) at a desired location was selected, zoomed in to the maximum (48×), and scanned with 100% 750 nm laser once. The laser-induced injury could be readily visualized in the bright field after scanning.

Kaede photoconversion

col1a2[Kaede] embryos at appropriate stages were anesthetized with tricaine and mounted in 0.8% low melting point agarose in a glass-bottom dish (MatTek). Photoconversion experiments were performed using the 405 nm laser and the 20× objective on the Olympus FV1200 confocal microscope. For photoconversion of large areas (∼5 to 6 somite region), 50% laser power was used to scan the desired ROI for two frames at a dwell time of 200 µs per pixel. For single cell photoconversions, 2% laser power was used to scan a small ROI (10×10 pixels) with the Tornado mode at a dwell time of 100 µs per pixel for a total of 1-2 s. After photoconversion, embryos were released from the agarose, transferred to fish water to recover in the dark, and analyzed at desired stages.

Cre-mediated lineage tracing

To obtain mosaic labeling, *col1a2:Gal4; UAS:Cre-ERT2; ubi:Switch* embryos were pulsed with 10 µM 4-hydroxytamoxifen (4-OHT) for 2-3 h at desired stages. After treatment, 4-OHT was rinsed off with fish water three times, and embryos were recovered in fish water for analysis at appropriate stages.

Single cell lineage tracing

Mosaic *col1a2*^Kaede^ embryos at appropriate stages were selected for single cell tracing experiments. Individual isolated *col1a2*^+^ MPCs were photoconverted to *Kaede*^red^. To ensure reliable cell tracing over time, a maximum of one cell per somite and four cells per embryo were photoconverted and traced. Immediately after photoconversion, muscle injury was introduced by laser ablation near one *Kaede*^red^ cell. Images were taken before and after the photoconversion and then every 24 h until 72 hpi to trace individual *Kaede*^red^ cells and their progeny. For quantification in Fig. 5D, distance was measured from the center of the photoconverted cell to the center of the muscle injury.

In situ hybridization and immunohistochemistry

Whole-mount *in situ* hybridization and antibody staining were performed according to the standard protocols (Thisse et al., 2004). The following antisense probes were used in this study: *cilp*, *col1a1a*, *col1a2*, *col5a1*, *kaede*, *myoD*, *myogenin*, *pax7a* (Seo et al., 1998), *postnb* and *sparc*. Double fluorescent *in situ* hybridizations were performed using different combinations of digoxigenin (DIG)- and dinitrophenyl (DNP)-labeled probes. For antibody staining, the following primary antibodies were used: rabbit polyclonal antibody to Kaede (1:1000; MBL, PM012), rabbit polyclonal antibody to RFP (1:1000; MBL, PM005) and mouse monoclonal antibody to Pax7 [1:10; Developmental Studies Hybridoma Bank (DSHB), PAX7-s]. For fluorescence detection of antibody labeling, appropriate Alexa Fluor-conjugated secondary antibodies (1:500; Thermo Fisher) were used.

Vibratome sectioning

Adult zebrafish were fixed in 4% paraformaldehyde (PFA) with 1% DMSO overnight at 4°C. After fixation, fish were washed in PBS and decalcified in 0.5 M EDTA for 3 days at room temperature. Following decalcification, the trunks were dissected, embedded in 20% gelatin and fixed overnight in 4% PFA at 4°C. Gelatin blocks were then washed with PBS and mounted in a Leica VT1000S vibratome to obtain transverse sections at 150 μm thick. Sections were mounted on slides in 50% glycerol for confocal imaging. Confocal tile scans were stitched together by the Olympus Fluoview software to generate the full view of the transverse section.

Cell ablation experiments

To ablate *col1a2*^+^ MPCs, *col1a2*^NTR-mCherry^ embryos at 2 dpf were treated with water (control group) or 5 mM metronidazole (MTZ, experimental group) for 24 h. Embryos were then washed with fish water two or three times and recovered at 28.5°C. To check ablation efficiency, embryos were fixed at 4 dpf and stained with anti-mCherry and anti-Pax7 antibodies. *Pax7*^+^ MPCs, including superficial MPCs in the dermomyotome and deep muscle fiber-associated cells, were counted for a 4-somite region of each embryo. To examine muscle regeneration, *mCherry*^+^ and *mCherry*^− embryos from a cross of *col1a2*^NTR-mCherry^ fish were treated with MTZ from 2 to 3 dpf, needle injured after the MTZ treatment, recovered, and fixed at 4 dpf for *in situ* analysis.

Time-lapse imaging and processing

Embryos were anesthetized with tricaine and embedded in 0.8% low melting point agarose on a glass-bottom dish (MatTek). Fish were imaged with an Olympus FV1200 confocal microscope using a 20× objective. For time-lapse imaging of muscle regeneration, embryos were first injured at 2 or 3 dpf by needle stabbing. Injured embryos were then imaged laterally starting at appropriate stages at 5- to 8-min intervals for 19-24 h. All the confocal images were analyzed and quantified using Fiji software (Schindelin et al., 2012). Brightness and contrast were adjusted for better visualization. To generate color-coded depth projections, confocal *z*-stacks were processed with Fiji using the 'temporal color code' function.

Quantification of muscle progenitor cells

To quantify the number of *col1a2*^+^ MPCs, *col1a2*^NTR-mCherry^ fish were stained with anti-Pax7 antibody at 2 dpf. Cells in each somite were counted based on *col1a2* expression and Pax7 staining: all *Pax7*^+^ cells, *Pax7*^+^*Col1a2*^+^ cells and *Pax7*^+^*Col1a2*^−^ cells. Note that xanthophores, which have strong Pax7 staining, were not counted. Each data point in the graph represents the average from five somites of one embryo. *Pax7*^+^*Col1a2*^+^ cells were further categorized according to their position in a somite: near the vertical myosepta (VM), near the horizontal myoseptum (HM) or in between somite boundaries (central). To quantify the number of fiber-associated MPCs, *col1a2*^NTR-mCherry^ fish were stained with anti-Pax7 antibody at 5 dpf. Cells deep in each somite between myofibers were counted based on *col1a2* expression and Pax7 staining: all *Pax7*^+^ cells, *Pax7*^+^*Col1a2*^+^ cells and *Pax7*^+^*Col1a2*^−^ cells.

Statistical analysis

All the graphs were generated in GraphPad Prism software. Data were plotted as mean±s.e.m. indicated. Significance between two samples was calculated by performing the Mann–Whitney *U*-test with two-tailed *P*-values: $*P<0.05$, $**P<0.01$, $***P<0.001$ and $****P<0.0001$.

Author contributions

Conceptualization: P.H.; Methodology: P.H., P.S., T.D.R., K.M.K., S.L.; Software: P.H., S.L.; Validation: P.H., P.S., T.D.R., K.M.K.; Formal analysis: P.H., P.S., T.D.R., K.M.K., S.L.; Investigation: P.H., P.S., T.D.R., K.M.K.; Resources: P.H., S.L.; Data curation: P.H., P.S., T.D.R., K.M.K.; Writing - original draft: P.H., P.S.; Writing - review & editing: P.H., P.S., T.D.R., K.M.K.; Visualization: P.H.; Supervision: P.H.; Project administration: P.H.; Funding acquisition: P.H.

Supplementary information

Supplementary information available online at
http://dev.biologists.org/lookup/doi/10.1242/dev.178400.supplemental

References

Akitake, C. M., Macurak, M., Halpern, M. E. and Goll, M. G. (2011). Transgenerational analysis of transcriptional silencing in zebrafish. *Dev. Biol.* **352**, 191-201. doi:10.1016/j.ydbio.2011.01.002

Ando, R., Hama, H., Yamamoto-Hino, M., Mizuno, H. and Miyawaki, A. (2002). An optical marker based on the UV-induced green-to-red photoconversion of a fluorescent protein. *Proc. Natl. Acad. Sci. USA* **99**, 12651-12656. doi:10.1073/pnas.202320599

Baghdadi, M. B., Castel, D., Machado, L., Fukada, S.-I., Birk, D. E., Relaix, F., Tajbakhsh, S. and Mourikis, P. (2018). Reciprocal signalling by Notch-Collagen V-CALCR retains muscle stem cells in their niche. *Nature* **557**, 714-718. doi:10.1038/s41586-018-0144-9

Bentzinger, C. F., Wang, Y. X., Dumont, N. A. and Rudnicki, M. A. (2013a). Cellular dynamics in the muscle satellite cell niche. *EMBO Rep.* **14**, 1062-1072. doi:10.1038/embor.2013.182

Bentzinger, C. F., Wang, Y. X., von Maltzahn, J., Soleimani, V. D., Yin, H. and Rudnicki, M. A. (2013b). Fibronectin regulates Wnt7a signaling and satellite cell expansion. *Cell Stem Cell* **12**, 75-87. doi:10.1016/j.stem.2012.09.015

Bentzinger, C. F., von Maltzahn, J., Dumont, N. A., Stark, D. A., Wang, Y. X., Nhan, K., Frenette, J., Cornelison, D. D. W. and Rudnicki, M. A. (2014). Wnt7a stimulates myogenic stem cell motility and engraftment resulting in improved muscle strength. *J. Cell Biol.* **205**, 97-111. doi:10.1083/jcb.201310035

Berberoglu, M. A., Gallagher, T. L., Morrow, Z. T., Talbot, J. C., Hromowyk, K. J., Tenente, I. M., Langenau, D. M. and Amacher, S. L. (2017). Satellite-like cells contribute to pax7-dependent skeletal muscle repair in adult zebrafish. *Dev. Biol.* **424**, 162-180. doi:10.1016/j.ydbio.2017.03.004

Bussmann, J. and Schulte-Merker, S. (2011). Rapid BAC selection for tol2-mediated transgenesis in zebrafish. *Development* 138, 4327-4332. doi:10.1242/dev.068080

Charvet, B., Malbouyres, M., Pagnon-Minot, A., Ruggiero, F. and Le Guellec, D. (2011). Development of the zebrafish myoseptum with emphasis on the myotendinous junction. *Cell Tissue Res.* 346, 439-449. doi:10.1007/s00441-011-1266-7

Christ, B. and Scaal, M. (2008). Formation and differentiation of avian somite derivatives. *Adv. Exp. Med. Biol.* 638, 1-41. doi:10.1007/978-0-387-09606-3_1

Curado, S., Stainier, D. Y. and Anderson, R. M. (2008). Nitroreductase-mediated cell/tissue ablation in zebrafish: a spatially and temporally controlled ablation method with applications in developmental and regeneration studies. *Nat. Protoc.* 3, 948-954. doi:10.1038/nprot.2008.58

Davison, J. M., Akitake, C. M., Goll, M. G., Rhee, J. M., Gosse, N., Baier, H., Halpern, M. E., Leach, S. D. and Parsons, M. J. (2007). Transactivation from Gal4-VP16 transgenic insertions for tissue-specific cell labeling and ablation in zebrafish. *Dev. Biol.* 304, 811-824. doi:10.1016/j.ydbio.2007.01.033

Devoto, S. H., Stoiber, W., Hammond, C. L., Steinbacher, P., Haslett, J. R., Barresi, M. J. F., Patterson, S. E., Adiarte, E. G. and Hughes, S. M. (2006). Generality of vertebrate developmental patterns: evidence for a dermomyotome in fish. *Evol. Dev.* 8, 101-110. doi:10.1111/j.1525-142X.2006.05079.x

Dumont, N. A., Bentzinger, C. F., Sincennes, M.-C. and Rudnicki, M. A. (2015). Satellite cells and skeletal muscle regeneration. *Comp. Physiol.* 5, 1027-1059. doi:10.1002/cphy.c140068

El Fahime, E., Torrente, Y., Caron, N. J., Bresolin, M. D. and Tremblay, J. P. (2000). In vivo migration of transplanted myoblasts requires matrix metalloproteinase activity. *Exp. Cell Res.* 258, 279-287. doi:10.1006/excr.2000.4962

Feng, X., Adiarte, E. G. and Devoto, S. H. (2006). Hedgehog acts directly on the zebrafish dermomyotome to promote myogenic differentiation. *Dev. Biol.* 300, 736-746. doi:10.1016/j.ydbio.2006.08.056

Fry, C. S., Kirby, T. J., Kosmac, K., McCarthy, J. J. and Peterson, C. A. (2017). Myogenic progenitor cells control extracellular matrix production by fibroblasts during skeletal muscle hypertrophy. *Cell Stem Cell* 20, 56-69. doi:10.1016/j.stem.2016.09.010

Gros, J., Manceau, M., Thomé, V. and Marcelle, C. (2005). A common somitic origin for embryonic muscle progenitors and satellite cells. *Nature* 435, 954-958. doi:10.1038/nature03572

Grueber, W. B. and Sagasti, A. (2010). Self-avoidance and tiling: mechanisms of dendrite and axon spacing. *Cold Spring Harb. Perspect Biol.* 2, a001750. doi:10.1101/cshperspect.a001750

Gurevich, D. B., Nguyen, P. D., Siegel, A. L., Ehrlich, O. V., Sonntag, C., Phan, J. M. N., Berger, S., Ratnayake, D., Hersey, L., Berger, J. et al. (2016). Asymmetric division of clonal muscle stem cells coordinates muscle regeneration in vivo. *Science* 353, aad9969. doi:10.1126/science.aad9969

Hammond, C. L., Hinits, Y., Osborn, D. P. S., Minchin, J. E. N., Tettamanti, G. and Hughes, S. M. (2007). Signals and myogenic regulatory factors restrict pax3 and pax7 expression to dermomyotome-like tissue in zebrafish. *Dev. Biol.* 302, 504-521. doi:10.1016/j.ydbio.2006.10.009

Higashijima, S., Okamoto, H., Ueno, N., Hotta, Y. and Eguchi, G. (1997). High-frequency generation of transgenic zebrafish which reliably express GFP in whole muscles or the whole body by using promoters of zebrafish origin. *Dev. Biol.* 192, 289-299. doi:10.1006/dbio.1997.8779

Hollway, G. E., Bryson-Richardson, R. J., Berger, S., Cole, N. J., Hall, T. E. and Currie, P. D. (2007). Whole-somite rotation generates muscle progenitor cell compartments in the developing zebrafish embryo. *Dev. Cell* 12, 207-219. doi:10.1016/j.devcel.2007.01.001

Huang, P., Xiong, F., Megason, S. G. and Schier, A. F. (2012). Attenuation of Notch and Hedgehog signaling is required for fate specification in the spinal cord. *PLoS Genet.* 8, e1002762. doi:10.1371/journal.pgen.1002762

Jockusch, H. and Voigt, S. (2003). Migration of adult myogenic precursor cells as revealed by GFP/nLacZ labelling of mouse transplantation chimeras. *J. Cell Sci.* 116, 1611-1616. doi:10.1242/jcs.00364

Kassar-Duchossoy, L., Giacone, E., Gayraud-Morel, B., Jory, A., Gomès, D. and Tajbakhsh, S. (2005). Pax3/Pax7 mark a novel population of primitive myogenic cells during development. *Genes Dev.* 19, 1426-1431. doi:10.1101/gad.345505

Kimmel, C. B., Ballard, W. W., Kimmel, S. R., Ullmann, B. and Schilling, T. F. (1995). Stages of embryonic development of the zebrafish. *Dev. Dyn.* 203, 253-310. doi:10.1002/aja.1002030302

Knappe, S., Zammit, P. S. and Knight, R. D. (2015). A population of Pax7-expressing muscle progenitor cells show differential responses to muscle injury dependent on developmental stage and injury extent. *Front. Aging Neurosci.* 7, 161. doi:10.3389/fnagi.2015.00161

Kuang, S., Kuroda, K., Le Grand, F. and Rudnicki, M. A. (2007). Asymmetric self-renewal and commitment of satellite stem cells in muscle. *Cell* 129, 999-1010. doi:10.1016/j.cell.2007.03.044

Le Guellec, D., Morvan-Dubois, G. and Sire, J.-Y. (2004). Skin development in bony fish with particular emphasis on collagen deposition in the dermis of the zebrafish (Danio rerio). *Int. J. Dev. Biol.* 48, 217-231. doi:10.1387/ijdb.15272388

Lepper, C., Partridge, T. A. and Fan, C.-M. (2011). An absolute requirement for Pax7-positive satellite cells in acute injury-induced skeletal muscle regeneration. *Development* 138, 3639-3646. doi:10.1242/dev.067595

Liu, N., Garry, G. A., Li, S., Bezprozvannaya, S., Sanchez-Ortiz, E., Chen, B., Shelton, J. M., Jaichander, P., Bassel-Duby, R. and Olson, E. N. (2017). A Twist2-dependent progenitor cell contributes to adult skeletal muscle. *Nat. Cell Biol.* 19, 202-213. doi:10.1038/ncb3477

Love, N. R., Chen, Y., Ishibashi, S., Kritsiligkou, P., Lea, R., Koh, Y., Gallop, J. L., Dorey, K. and Amaya, E. (2013). Amputation-induced reactive oxygen species are required for successful Xenopus tadpole tail regeneration. *Nat. Cell Biol.* 15, 222-228. doi:10.1038/ncb2659

Ma, R. C., Jacobs, C. T., Sharma, P., Kocha, K. M. and Huang, P. (2018). Stereotypic generation of axial tenocytes from bipartite sclerotome domains in zebrafish. *PLoS Genet.* 14, e1007775. doi:10.1371/journal.pgen.1007775

Mosimann, C., Kaufman, C. K., Li, P., Pugach, E. K., Tamplin, O. J. and Zon, L. I. (2011). Ubiquitous transgene expression and Cre-based recombination driven by the ubiquitin promoter in zebrafish. *Development* 138, 169-177. doi:10.1242/dev.059345

Murphy, M. M., Lawson, J. A., Mathew, S. J., Hutcheson, D. A. and Kardon, G. (2011). Satellite cells, connective tissue fibroblasts and their interactions are crucial for muscle regeneration. *Development* 138, 3625-3637. doi:10.1242/dev.064162

Nguyen, P. D., Gurevich, D. B., Sonntag, C., Hersey, L., Alaei, S., Nim, H. T., Siegel, A., Hall, T. E., Rossello, F. J., Boyd, S. E. et al. (2017). Muscle stem cells undergo extensive clonal drift during tissue growth via Meox1-mediated induction of G2 cell-cycle arrest. *Cell Stem Cell* 21, 107-119.e106. doi:10.1016/j.stem.2017.06.003

Niethammer, P., Grabher, C., Look, A. T. and Mitchison, T. J. (2009). A tissue-scale gradient of hydrogen peroxide mediates rapid wound detection in zebrafish. *Nature* 459, 996-999. doi:10.1038/nature08119

Pallafacchina, G., François, S., Regnault, B., Czarny, B., Dive, V., Cumano, A., Montarras, D. and Buckingham, M. (2010). An adult tissue-specific stem cell in its niche: a gene profiling analysis of in vivo quiescent and activated muscle satellite cells. *Stem Cell Res.* 4, 77-91. doi:10.1016/j.scr.2009.10.003

Pan, Y. A., Freundlich, T., Weissman, T. A., Schoppik, D., Wang, X. C., Zimmerman, S., Ciruna, B., Sanes, J. R., Lichtman, J. W. and Schier, A. F. (2013). Zebrabow: multispectral cell labeling for cell tracing and lineage analysis in zebrafish. *Development* 140, 2835-2846. doi:10.1242/dev.094631

Pipalia, T. G., Koth, J., Roy, S. D., Hammond, C. L., Kawakami, K. and Hughes, S. M. (2016). Cellular dynamics of regeneration reveals role of two distinct Pax7 stem cell populations in larval zebrafish muscle repair. *Dis. Model. Mech.* 9, 671-684. doi:10.1242/dmm.022251

Pisharath, H., Rhee, J. M., Swanson, M. A., Leach, S. D. and Parsons, M. J. (2007). Targeted ablation of beta cells in the embryonic zebrafish pancreas using E. coli nitroreductase. *Mech. Dev.* 124, 218-229. doi:10.1016/j.mod.2006.11.005

Ralliere, C., Fretaud, M., Thermes, V. and Rescan, P.-Y. (2015). CILP1 is dynamically expressed in the developing musculoskeletal system of the trout. *Int. J. Dev. Biol.* 59, 505-509. doi:10.1387/ijdb.150136pr

Ratnayake, D. and Currie, P. D. (2017). Stem cell dynamics in muscle regeneration: insights from live imaging in different animal models. *BioEssays* 39, 1700011. doi:10.1002/bies.201700011

Rayagiri, S. S., Ranaldi, D., Raven, A., Mohamad Azhar, N. I. F., Lefebvre, O., Zammit, P. S. and Borycki, A.-G. (2018). Basal lamina remodeling at the skeletal muscle stem cell niche mediates stem cell self-renewal. *Nat. Commun.* 9, 1075. doi:10.1038/s41467-018-03425-3

Relaix, F., Rocancourt, D., Mansouri, A. and Buckingham, M. (2005). A Pax3/Pax7-dependent population of skeletal muscle progenitor cells. *Nature* 435, 948-953. doi:10.1038/nature03594

Rescan, P. Y., Ralliere, C., Chauvigné, F. and Cauty, C. (2005). Expression patterns of collagen I (alpha1) encoding gene and muscle-specific genes reveal that the lateral domain of the fish somite forms a connective tissue surrounding the myotome. *Dev. Dyn.* 233, 605-611. doi:10.1002/dvdy.20337

Roy, S. D., Williams, V. C., Pipalia, T. G., Li, K., Hammond, C. L., Knappe, S., Knight, R. D. and Hughes, S. M. (2017). Myotome adaptability confers developmental robustness to somitic myogenesis in response to fibre number alteration. *Dev. Biol.* 431, 321-335. doi:10.1016/j.ydbio.2017.08.029

Sacco, A., Doyonnas, R., Kraft, P., Vitorovic, S. and Blau, H. M. (2008). Self-renewal and expansion of single transplanted muscle stem cells. *Nature* 456, 502-506. doi:10.1038/nature07384

Saclier, M., Yacoub-Youssef, H., Mackey, A. L., Arnold, L., Ardjoune, H., Magnan, M., Sailhan, F., Chelly, J., Pavlath, G. K., Mounier, R. et al. (2013). Differentially activated macrophages orchestrate myogenic precursor cell fate during human skeletal muscle regeneration. *Stem Cells* 31, 384-396. doi:10.1002/stem.1288

Saga, Y. and Takeda, H. (2001). The making of the somite: molecular events in vertebrate segmentation. *Nat. Rev. Genet.* 2, 835-845. doi:10.1038/35098552

Sagar, Pröls, F., Wiegreffe, C. and Scaal, M. (2015). Communication between distant epithelial cells by filopodia-like protrusions during embryonic development. *Development* 142, 665-671. doi:10.1242/dev.115964

DEVELOPMENT

Sambasivan, R., Yao, R., Kissenpfennig, A., Van Wittenberghe, L., Paldi, A., Gayraud-Morel, B., Guenou, H., Malissen, B., Tajbakhsh, S. and Galy, A. (2011). Pax7-expressing satellite cells are indispensable for adult skeletal muscle regeneration. *Development* **138**, 3647-3656. doi:10.1242/dev.067587

Scaal, M. and Christ, B. (2004). Formation and differentiation of the avian dermomyotome. *Anat. Embryol.* **208**, 411-424. doi:10.1007/s00429-004-0417-y

Scharner, J. and Zammit, P. S. (2011). The muscle satellite cell at 50: the formative years. *Skelet Muscle* **1**, 28. doi:10.1186/2044-5040-1-28

Schienda, J., Engleka, K. A., Jun, S., Hansen, M. S., Epstein, J. A., Tabin, C. J., Kunkel, L. M. and Kardon, G. (2006). Somitic origin of limb muscle satellite and side population cells. *Proc. Natl. Acad. Sci. USA* **103**, 945-950. doi:10.1073/pnas.0510164103

Schindelin, J., Arganda-Carreras, I., Frise, E., Kaynig, V., Longair, M., Pietzsch, T., Preibisch, S., Rueden, C., Saalfeld, S., Schmid, B. et al. (2012). Fiji: an open-source platform for biological-image analysis. *Nat. Methods* **9**, 676-682. doi:10.1038/nmeth.2019

Scott, E. K., Mason, L., Arrenberg, A. B., Ziv, L., Gosse, N. J., Xiao, T., Chi, N. C., Asakawa, K., Kawakami, K. and Baier, H. (2007). Targeting neural circuitry in zebrafish using GAL4 enhancer trapping. *Nat. Methods* **4**, 323-326. doi:10.1038/nmeth1033

Seger, C., Hargrave, M., Wang, X., Chai, R. J., Elworthy, S. and Ingham, P. W. (2011). Analysis of Pax7 expressing myogenic cells in zebrafish muscle development, injury, and models of disease. *Dev. Dyn.* **240**, 2440-2451. doi:10.1002/dvdy.22745

Seo, H.-C., Saetre, B. O., Håvik, B., Ellingsen, S. and Fjose, A. (1998). The zebrafish Pax3 and Pax7 homologues are highly conserved, encode multiple isoforms and show dynamic segment-like expression in the developing brain. *Mech. Dev.* **70**, 49-63. doi:10.1016/S0925-4773(97)00175-5

Siegel, A. L., Atchison, K., Fisher, K. E., Davis, G. E. and Cornelison, D. D. (2009). 3D timelapse analysis of muscle satellite cell motility. *Stem Cells* **27**, 2527-2538. doi:10.1002/stem.178

Stellabotte, F. and Devoto, S. H. (2007). The teleost dermomyotome. *Dev. Dyn.* **236**, 2432-2443. doi:10.1002/dvdy.21253

Stellabotte, F., Dobbs-McAuliffe, B., Fernández, D. A., Feng, X. and Devoto, S. H. (2007). Dynamic somite cell rearrangements lead to distinct waves of myotome growth. *Development* **134**, 1253-1257. doi:10.1242/dev.000067

Suster, M. L., Kikuta, H., Urasaki, A., Asakawa, K. and Kawakami, K. (2009). Transgenesis in zebrafish with the tol2 transposon system. *Methods Mol. Biol.* **561**, 41-63. doi:10.1007/978-1-60327-019-9_3

Thisse, B., Heyer, V., Lux, A., Alunni, V., Degrave, A., Seiliez, I., Kirchner, J., Parkhill, J.-P. and Thisse, C. (2004). Spatial and temporal expression of the zebrafish genome by large-scale in situ hybridization screening. *Methods Cell Biol.* **77**, 505-519. doi:10.1016/S0091-679X(04)77027-2

Tierney, M. T., Gromova, A., Sesillo, F. B., Sala, D., Spenlé, C., Orend, G. and Sacco, A. (2016). Autonomous extracellular matrix remodeling controls a progressive adaptation in muscle stem cell regenerative capacity during development. *Cell Rep.* **14**, 1940-1952. doi:10.1016/j.celrep.2016.01.072

Urciuolo, A., Quarta, M., Morbidoni, V., Gattazzo, F., Molon, S., Grumati, P., Montemurro, F., Tedesco, F. S., Blaauw, B., Cossu, G. et al. (2013). Collagen VI regulates satellite cell self-renewal and muscle regeneration. *Nat. Commun.* **4**, 1964. doi:10.1038/ncomms2964

Webster, M. T., Manor, U., Lippincott-Schwartz, J. and Fan, C. M. (2016). Intravital imaging reveals ghost fibers as architectural units guiding myogenic progenitors during regeneration. *Cell Stem Cell* **18**, 243-252. doi:10.1016/j.stem.2015.11.005

Westerfield, M. (2000). *The Zebrafish Book: A Guide for the Laboratory Use of Zebrafish (Danio Rerio)*, 4 edn. University of Oregon.
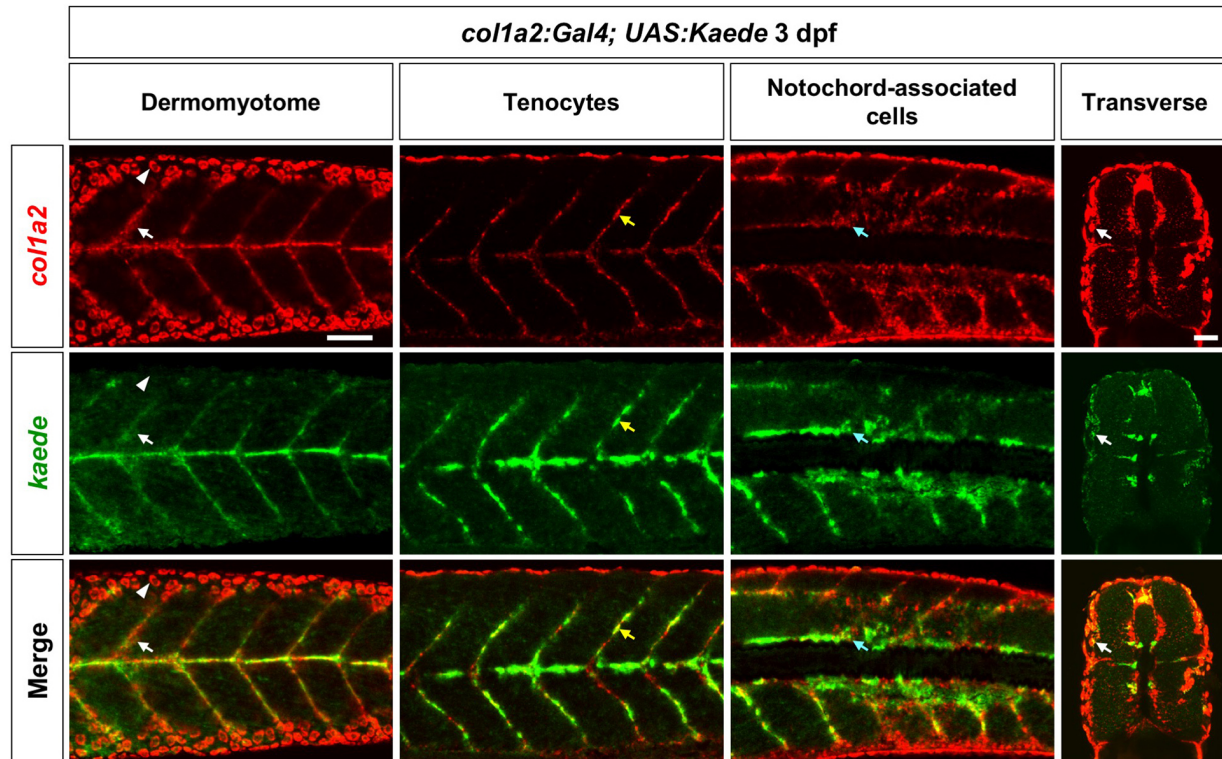
DEVELOPMENT

Figure S1. Validation of the *col1a2^{Kaede}* line. Double fluorescent in situ hybridization using *kaede* and *col1a2* probes were performed in *col1a2^{Kaede}* embryos at 3 dpf. Co-expression of *kaede* (green) and the endogenous *col1a2* (red) can be observed in dermomyotome cells (white arrows), tenocytes along the vertical myoseptum (yellow arrows), and deep interstitial cells around the notochord (cyan arrows). Note that *col1a2^{Kaede}* was not expressed in the epidermis (arrowheads) as *col1a2*. *n* = 19 embryos. Scale bar: 50 μm.
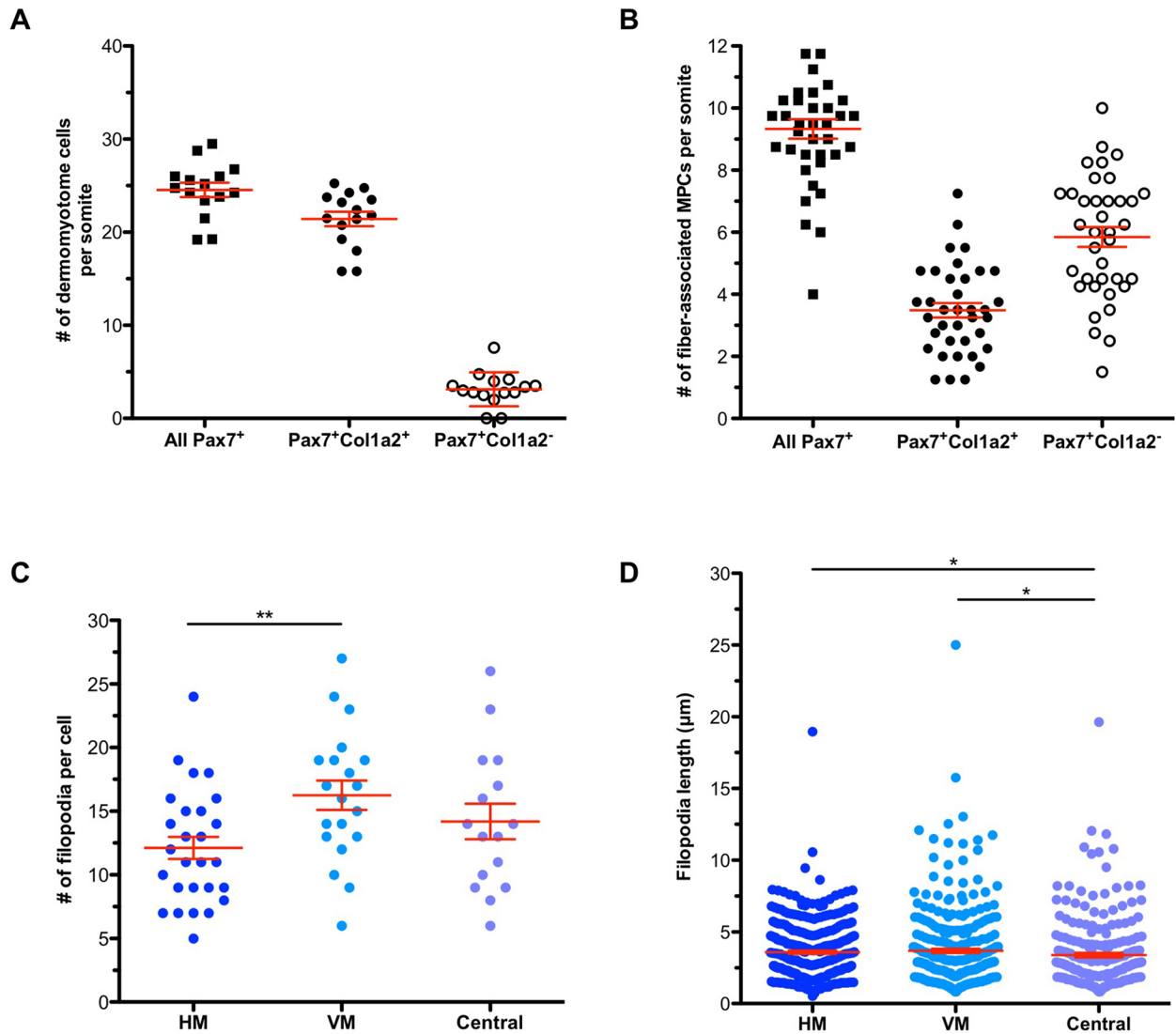
Figure S2. Characterization of *col1a2⁺* MPCs. (A) Quantification of dermomyotome cells per somite in *col1a2^(NTR-mCherry)* fish stained with anti-Pax7 antibody at 2 dpf (*n* = 15 embryos). (B) Quantification of fiber-associated MPCs per somite in *col1a2^(NTR-mCherry)* fish stained with anti-Pax7 antibody at 5 dpf (*n* = 37 embryos). (C-D) Single *col1a2⁺* MPCs in mosaic *col1a2^(Kaede)* fish were imaged to quantify the number (C) and length (D) of their filopodia (*n* = 36 embryos). HM: 27 cells; VM: 20 cells; Central: 16 cells. All data are plotted with mean ± SEM indicated. Statistics: Mann-Whitney *U* test. Asterisks representation: p-value < 0.05 (*) and p-value < 0.01 (**).
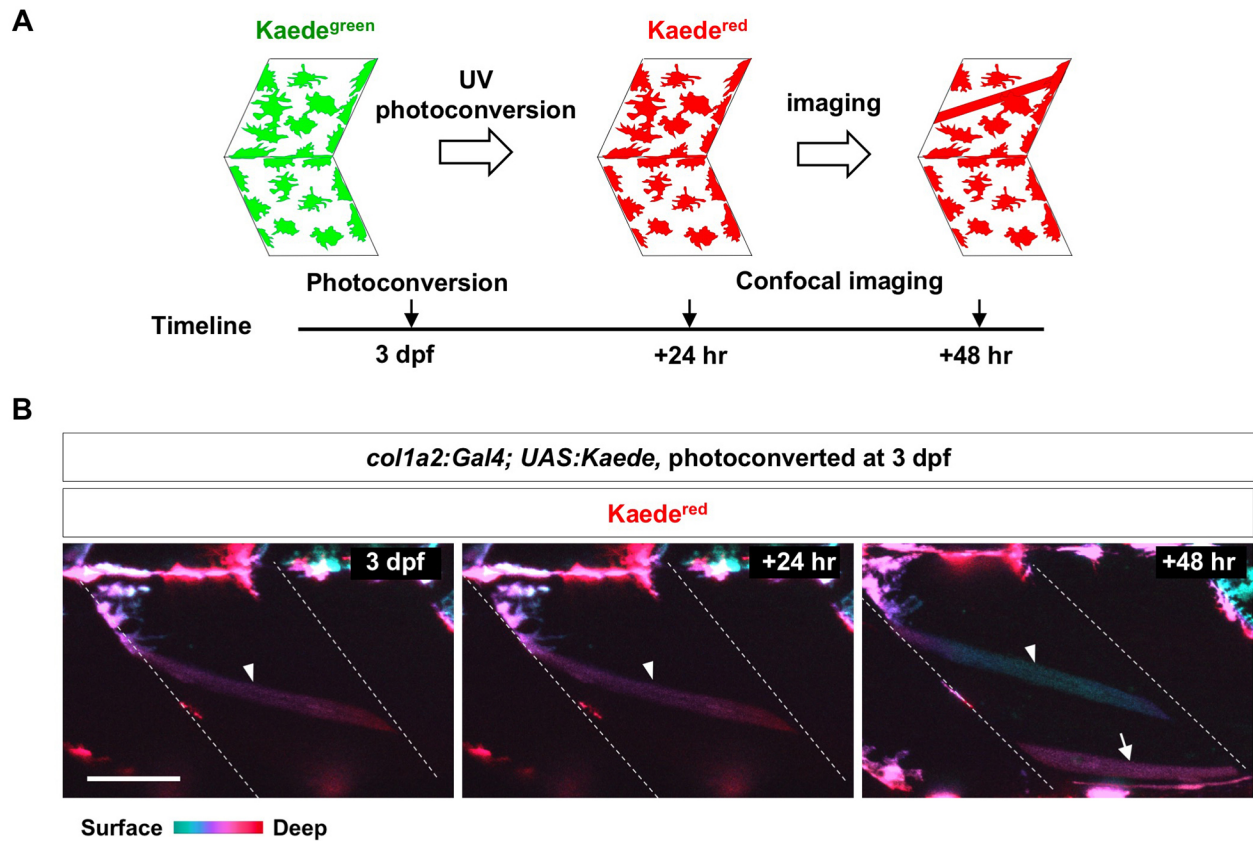
Figure S3. *col1a2+* cells contribute to muscle growth. (A) Schematics of photoconversion-based lineage tracing. (B) *col1a2Kaede* embryos were photoconverted at 3 dpf, and imaged at indicated time points. Color coded depth projections (green corresponds to superficial slices, while red denotes deep slices) of converted *Kaedered* showed that new *Kaedered* muscle fibers (arrow) emerged at 48-hour post conversion. An existing muscle fiber present through all 3 time points is indicated by arrowheads. *n* = 15 embryos. Scale bar: 50 *μ*m.
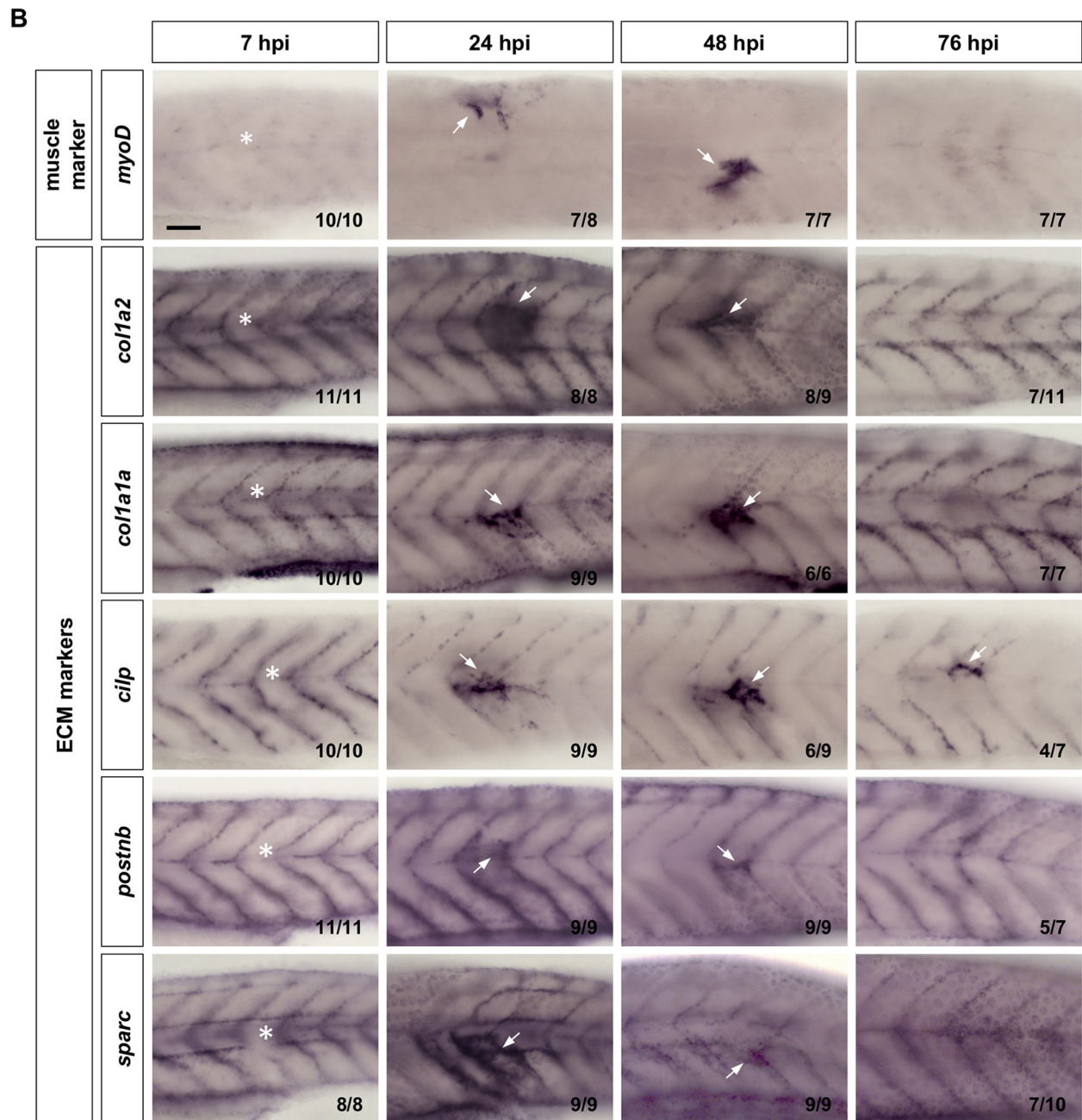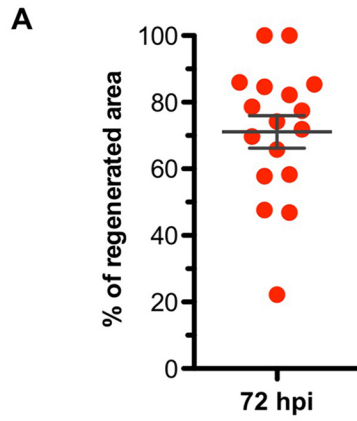
Figure S4. ECM molecules are upregulated during muscle regeneration. (A) Quantification of *col1a2*$^+$ MPC contribution to muscle regeneration in *col1a2*$^{NTR\text{-}mCherry}$*; α-actin:GFP* embryos at 72 hpi. The corresponding experiment is shown in Figure 4A. The percentage of contribution was calculated by dividing the area of *mCherry*$^+$ muscle fibers at the injury site by the total regenerated area marked by slightly elevated *α-actin:GFP* expression. Data are plotted with mean ± SEM indicated. *n* = 17 embryos. (B) Wild-type embryos were needle stabbed to injure a somite near the end of yolk extension (asterisks) at 3dpf, and fixed at 7, 24, 48, and 76 hpi. Embryos were then stained with the myogenic marker (*myoD*) and ECM markers (*col1a2, col1a1a, cilp, postnb,* and *sparc*). All markers showed upregulation at the site of injury starting from 24 hpi (arrows). Representative images are shown with the *n* number indicated for each staining. Scale bar: 50 *μ*m.
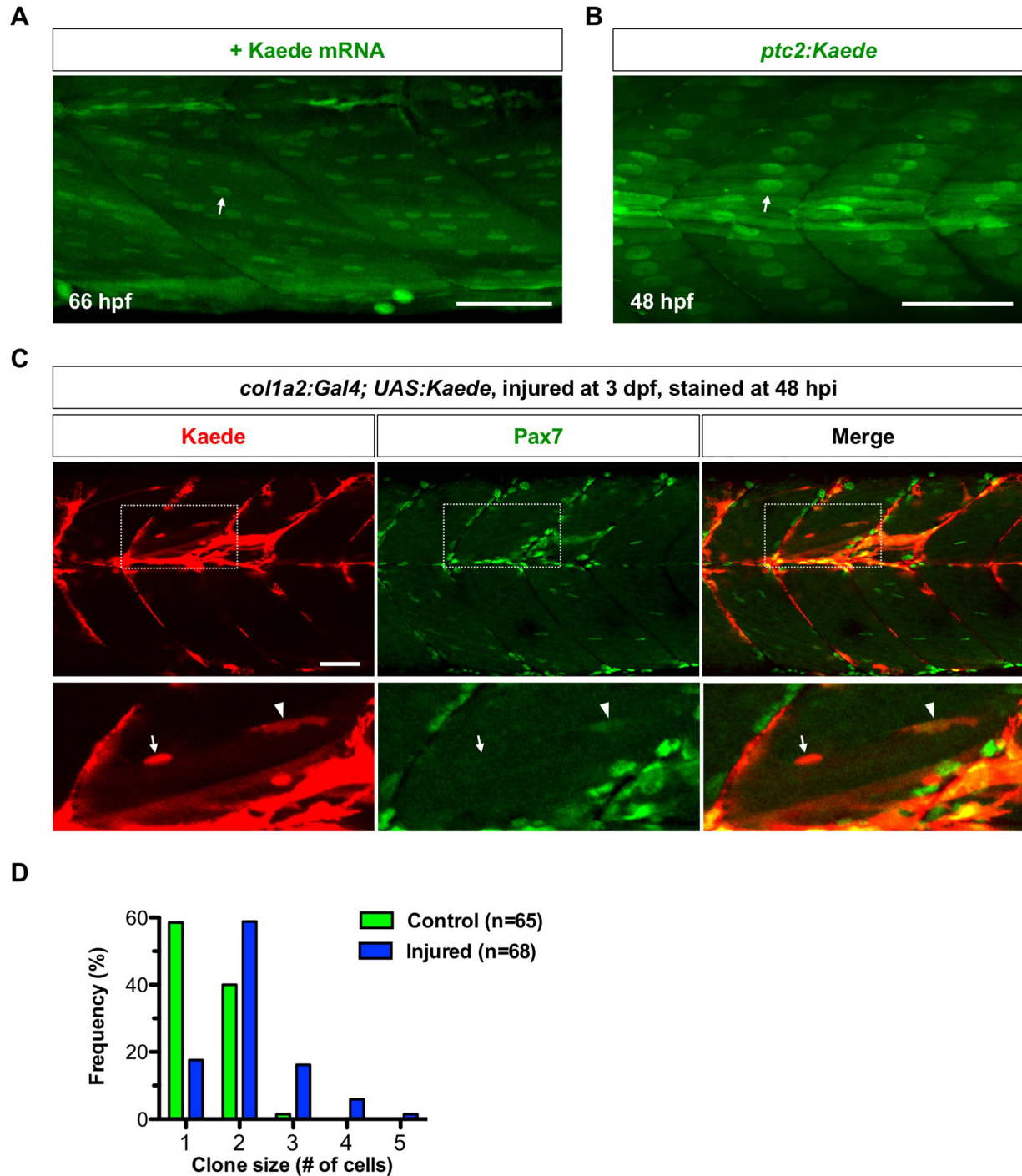
Figure S5. Kaede protein is preferentially localized in nuclei of muscle fibers. (A) Wild-type embryos were injected with Kaede mRNA, and imaged at 66 hpf. Kaede protein (green) is preferentially localized in the nuclei of muscle fibers (arrow). n = 40 embryos. (B) Kaede protein (green) is concentrated in the nuclei of slow myofibers (arrow) in *ptc2:Kaede* embryos at 48 hpf. n = 40 embryos. (C) *col1a2^Kaede* embryos were injured at 3 dpf, and stained at 48 hpi

with the anti-Pax7 antibody (green). *Kaede*^{+} cells (red) contributed to muscle regeneration (boxed regions). The expanded views show that newly formed muscle fiber displayed strong Kaede expression in the nucleus (arrows), which was not labelled by Pax7. By contrast, a small elongated *Kaede*[+] cell between muscle fibers was Pax7 positive (arrowheads). *n* = 11 embryos. (D) Quantification of clone size in single cell clonal analysis described in Fig 5. *col1a2*[+] MPCs under the injury condition (blue, n=68) tend to generate larger clones compared to MPCs in the wild-type condition (green, n=65). Scale bars: 50 *μ*m.

A

B
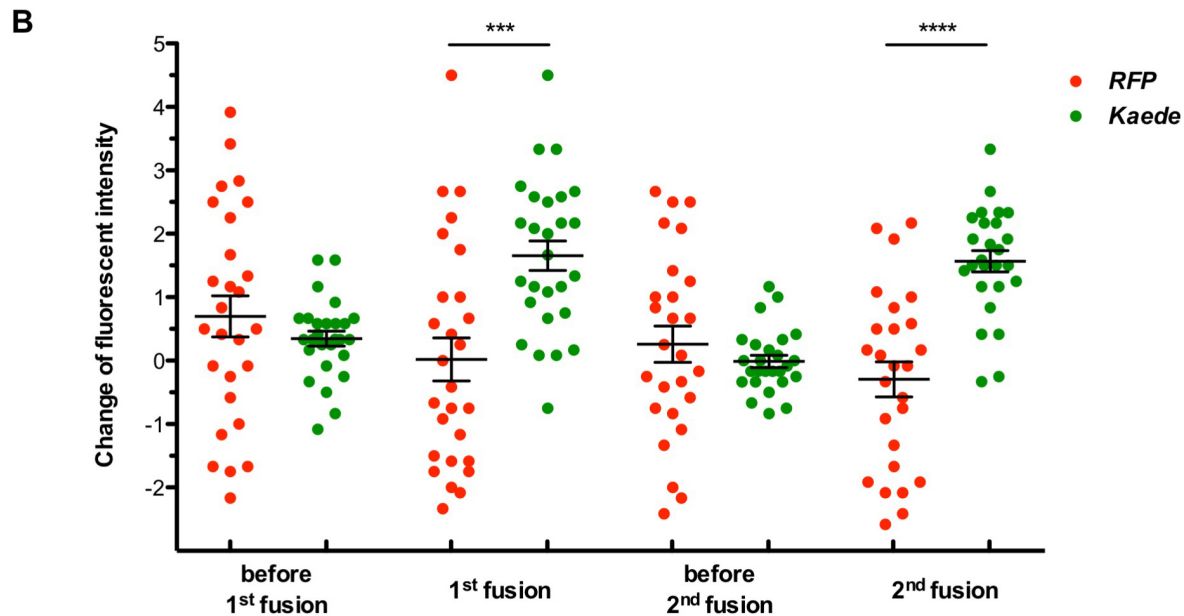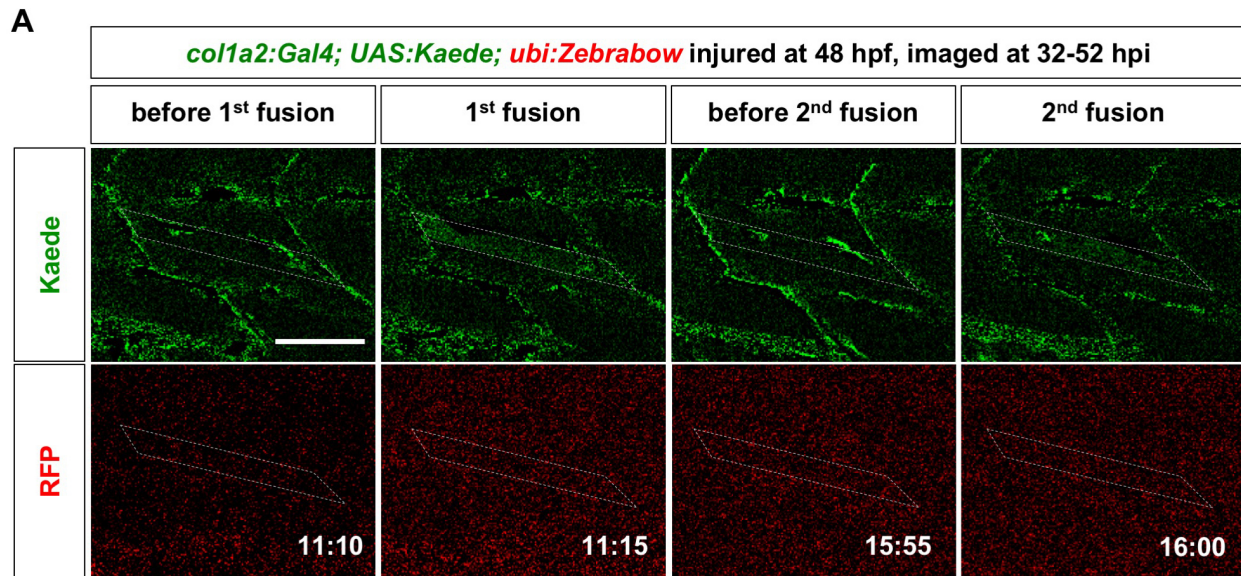
Figure S6. Quantification of sequential muscle fusion of *col1a2+* sibling cells. *col1a2^{Kaede}*; *ubi:Zebrabow* embryos were injured at 48 hpf, and imaged from 32 to 52 hpi. The same experiment is also shown in Figure 6E and Movie 6. (A) Image quantification. Change in fluorescent intensity at each time point was generated by subtracting the fluorescent intensity of corresponding channels at the previous time point (5 minutes earlier). Note that negative pixel values after image processing were set to zero. The muscle fiber that *col1a2+* sibling cells fused to is indicated by dotted lines. The increase of Kaede intensity but not the RFP signal in the muscle fiber can be observed at 11:15 (1st fusion event) and 16:00 (2nd fusion event). (B)

Quantification of fluorescence change before and after cell fusions. Small ROIs within the outlined muscle fiber were measured for fluorescent intensity at different time points ($n = 27$ for the 1st fusion event and $n = 26$ for the 2nd fusion event). Change in fluorescent intensity for each ROI in each channel was calculated and plotted for each time point. For example, change in fluorescent intensity for a given ROI at the 1st fusion (11:15) was generated by subtracting the fluorescent intensity at 11:10 from the intensity at 11:15. Significant increase in Kaede intensity but not the RFP signal in the muscle fiber can be observed at 11:15 (1st fusion event) and 16:00 (2nd fusion event), suggesting fusion events between a *Kaede*+ MPC and a muscle fiber. All data are plotted with mean ± SEM indicated. Statistics: Mann-Whitney *U* test. Asterisks representation: p-value < 0.001 (***) and p-value < 0.0001 (****). Scale bar: 50 *μ*m.
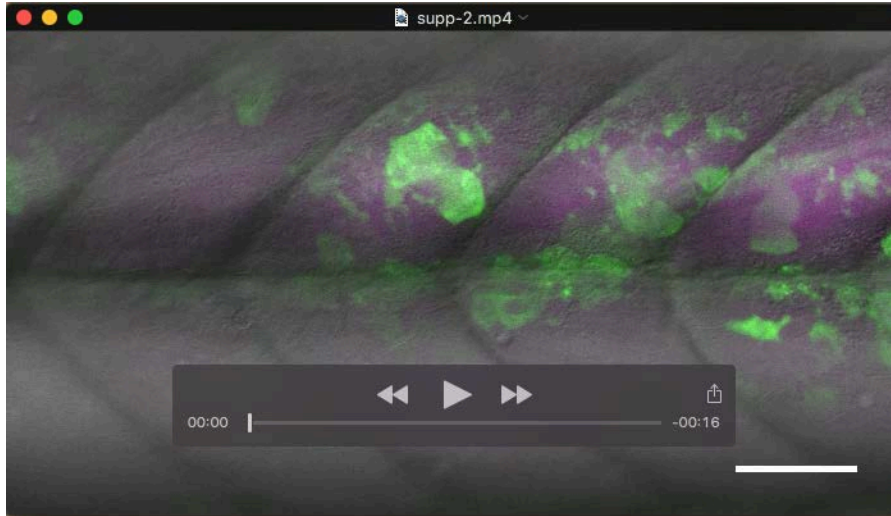
**Movie 1. Expression pattern of the _col1a2^{NTR-mCherry}_ line.** A confocal z-stack of _col1a2:Gal4; UAS:NTR-mCherry; α-actin:GFP_ embryos at 3 dpf shows mCherry expression (green) in dermomyotome cells, some muscle fibers, tenocytes and notochord-associated cells (arrows). Muscle fibers are labeled with _α-actin:GFP_ (magenta). Scale bar: 50 μm.
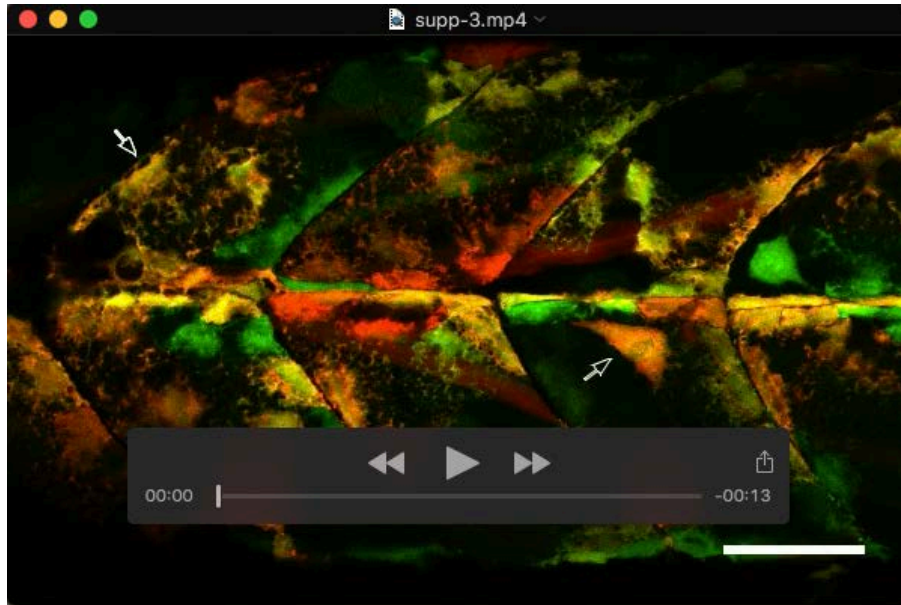
Movie 2. Dynamics *col1a2⁺* MPCs in quiescent state. *col1a2:Gal4; UAS:NTR-mCherry; UAS:Kaede* embryos were imaged at 2 dpf for 7.9 hours. *col1a2⁺* MPCs cover the surface of the somite. When a *col1a2⁺* MPC divides, daughter cells reclaim the same surface area soon after the division. Five different cell divisions are indicated by arrows. Representative snapshots are shown in Figure 2D. Scale bars: 50 *µ*m.
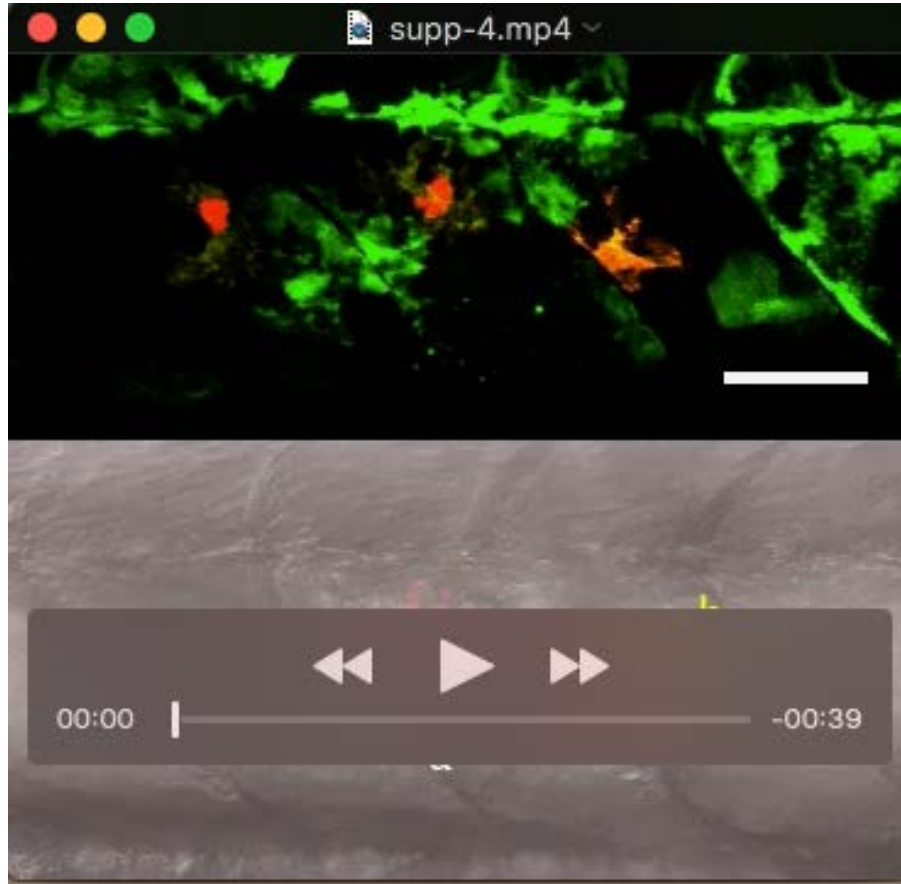
Movie 3. Dynamics *col1a2*⁺ MPCs in injured condition. *col1a2^Kaede* embryos were injured, photoconverted at 59 hpf, and then imaged over 23 hours (0-23 hpi). Cells "a" and "b" were within the injured area while the cell "c" was in the uninjured area. Cell "a" (white arrows) maintained the ramified morphology, and divided once at 7 hpi generating two daughter cells with similar morphologies. By contrast, cell "b" (yellow arrows) extended to form an elongated morphology (arrowheads), and divided once at 16 hpi generating two polarized daughter cells. Cell "c" (cyan arrows) did not divide and remained its ramified morphology. Representative snapshots of the injured area (cell a and b) are shown in Figure 6B. Scale bar: 50 *μ*m.
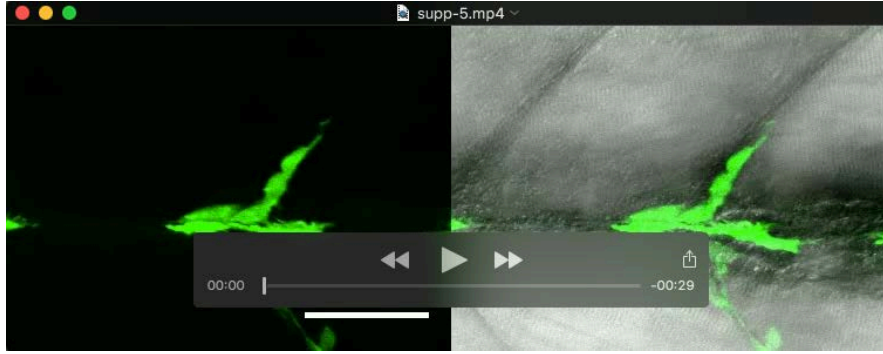
Movie 4. Generation of new muscle fibers by cell fusion. *col1a2^Kaede* fish was injured at 3 dpf and imaged from 29 hpi onwards. A *Kaede^+* MPC (arrows) near the injury site elongated at 34 hpi (white arrowheads), formed protrusions at 39 hpi, and fused with a neighboring muscle fiber at 40 hpi. The newly formed muscle fiber can be identified by the weak Kaede expression throughout the muscle fiber and the strong Kaede expression in the nucleus (yellow arrowheads). Representative snapshots are shown in Figure 6D. Scale bar: 50 *μ*m.
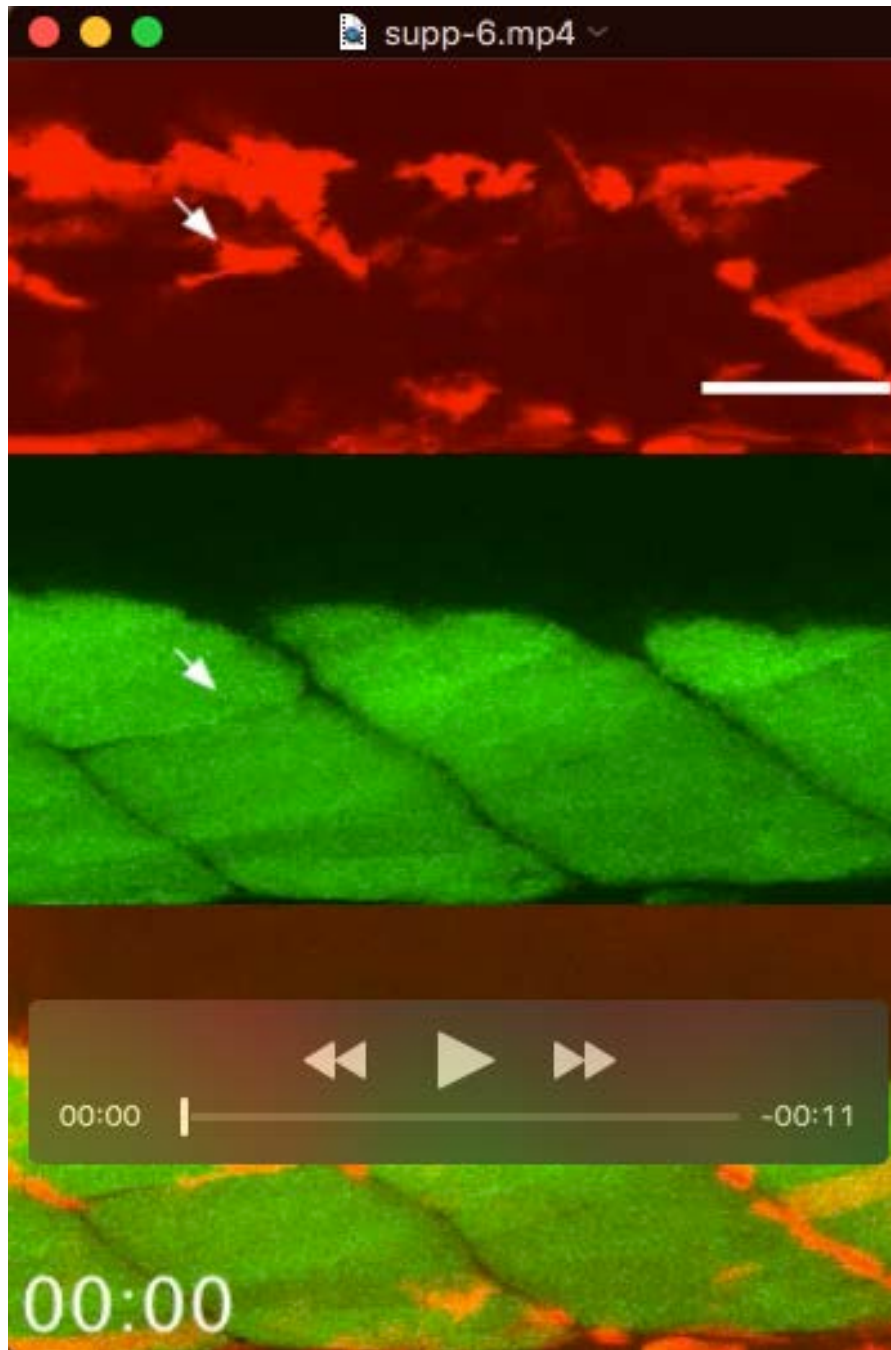
Movie 5. Generation of new muscle fibers by cell fusion. *col1a2^NTR-mCherry*; *α-actin:GFP* embryos were injured at 79 hpf and imaged from 24 to 36 hpi. The red channel (*col1a2^NTR-mCherry*), the green channel (*α-actin:GFP*), and the merged images are shown with time stamps indicated in the hh:mm format. A *mCherry⁺* MPC (arrows) near the injury site elongated and fused with a neighboring muscle fiber between 07:07 and 07:14. The fusion event was evident by the spreading of the mCherry signal in the muscle fiber and the mCherry signal in the nucleus (arrowheads) remained visible until the end of the movie at 12:15. A total of 23 fusion events were observed in movies from 12 embryos. Scale bar: 50 *µm*.
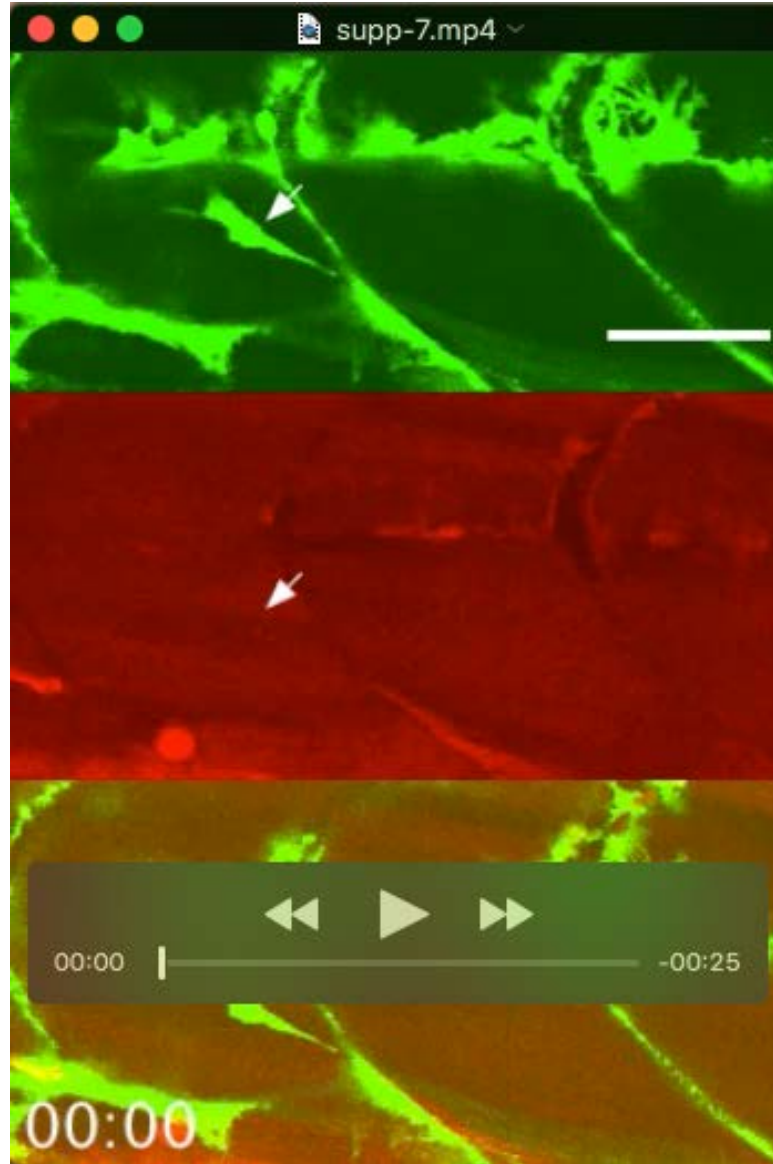
Movie 6. Sequential fusions of sibling cells derived from *col1a2*+ MPCs. *col1a2^Kaede^;*
ubi:Zebrabow embryos were injured at 48 hpf, and imaged from 32 to 52 hpi. Representative
snapshots and image quantification are shown in Figures 6E and S6, respectively. The green
channel (*col1a2^Kaede^*), the red channel (*ubi:Zebrabow*) and the merged images are shown with
time stamps indicated in the hh:mm format. Note that *Kaede*+ MPCs showed almost no RFP
expression compared to muscle cells. A *Kaede*+ cell (white arrows) divided between 00:55 and
01:00. The anterior daughter cell (cyan arrows) fused with a muscle fiber between 11:10 and
11:15, while the posterior daughter cell (yellow arrows) fused with the same muscle fiber
between 15:55 and 16:00. Concentrated Kaede expression in the nucleus after cell fusion was
clearly visible (arrowheads of corresponding colors). A total of 31 fusion events were observed
in movies of 12 embryos. Scale bar: 50 *μ*m.